Molecular Therapy
Original Article

Comprehensive Molecular Profiles of Functionally Effective MSC-Derived Extracellular Vesicles in Immunomodulation

Hyemee Kim,[1,6] Min Joung Lee,[2,6] Eun-Hye Bae,[1,6] Jin Suk Ryu,[3,6] Gagandeep Kaur,[1] Hyeon Ji Kim,[3] Jun Yeob Kim,[3] Heather Barreda,[1] Sung Youn Jung,[4] Jong Min Choi,[4] Taeko Shigemoto-Kuroda,[1] Joo Youn Oh,[3,5] and Ryang Hwa Lee[1]

[1]Department of Molecular and Cellular Medicine, Institute for Regenerative Medicine, College of Medicine, Texas A&M University, 1114 TAMU, 206 Olsen Boulevard, College Station, TX 77845, USA; [2]Department of Ophthalmology, Hallym University Sacred Heart Hospital, 22, Gwanpyeong-ro 170beon-gil, Dongan-gu, Anyang-si, Gyeonggi-do 14068, Korea; [3]Laboratory of Ocular Regenerative Medicine and Immunology, Biomedical Research Institute, Seoul National University Hospital, 101 Daehak-ro, Jongno-gu, Seoul, Korea; [4]Department of Molecular and Cellular Biology, Baylor College of Medicine, Houston, TX 77030, USA; [5]Department of Ophthalmology, Seoul National University College of Medicine, 103 Daehak-ro, Jongno-gu, Seoul 03080, Korea

Accumulating evidence indicates that mesenchymal stem/stromal cell-derived extracellular vesicles (MSC-EVs) exhibit immunomodulatory effects by delivering therapeutic RNAs and proteins; however, the molecular mechanism underlying the EV-mediated immunomodulation is not fully understood. In this study, we found that EVs from early-passage MSCs had better immunomodulatory potency than did EVs from late-passage MSCs in T cell receptor (TCR)- or Toll-like receptor 4 (TLR4)-stimulated splenocytes and in mice with ocular Sjögren's syndrome. Moreover, MSC-EVs were more effective when produced from 3D culture of the cells than from the conventional 2D culture. Comparative molecular profiling using proteomics and microRNA sequencing revealed the enriched factors in MSC-EVs that were functionally effective in immunomodulation. Among them, manipulation of transforming growth factor β1 (TGF-β1), pentraxin 3 (PTX3), let-7b-5p, or miR-21-5p levels in MSCs significantly affected the immunosuppressive effects of their EVs. Furthermore, there was a strong correlation between the expression levels of TGF-β1, PTX3, let-7b-5p, or miR-21-5p in MSC-EVs and their suppressive function. Therefore, our comparative strategy identified TGF-β1, PTX3, let-7b-5p, or miR-21-5p as key molecules mediating the therapeutic effects of MSC-EVs in autoimmune disease. These findings would help understand the molecular mechanism underlying EV-mediated immunomodulation and provide functional biomarkers of EVs for the development of robust EV-based therapies.

INTRODUCTION

Accumulating evidence indicates that extracellular vesicles (EVs) derived from mesenchymal stem/stromal cells (MSCs) recapitulate a broad range of the therapeutic effects shown by MSC treatment.[1,2] In a previous study, our group directly compared the therapeutic efficacy of MSCs with their EVs in autoimmune disease models for type 1 diabetes and experimental autoimmune uveoretinitis and found that MSC-derived EVs (MSC-EVs) were as effective as their parent MSCs in alleviating immune responses.[3] In a subsequent study, we also observed that therapeutic effects of EVs produced from induced pluripotent stem cell (iPSC)-derived MSCs were similar to bone marrow MSC-EVs in mice with dry mouth due to Sjögren's syndrome.[4] Consistent with our findings, several groups reported on the immunomodulatory effects of EVs from umbilical cord blood-derived and adipose-derived MSCs.[5–9]

Mechanistically, our previous study showed that MSC-EVs suppressed the activation of T cells and antigen-presenting cells (APCs), thereby inhibiting the development of T helper 1 (Th1) and Th17 cells.[3] Similarly, other studies revealed that MSC-EVs promoted the apoptotic activity toward activated T cells in splenocytes and induced the secretion of immunomodulatory cytokines such as interleukin (IL)-10 and transforming growth factor (TGF)-β, which were capable of inhibiting autoreactive lymphocyte proliferation and inducing regulatory T cell (Treg) generation.[10–14] Also, EVs have been shown to suppress macrophage activation[15,16] and induce M2-type macrophage polarization.[7,17,18] Therefore, the data strongly support the notion that MSC-EVs exert immunosuppressive effects on immune cells and in mice with immune-mediated diseases.

Received 12 December 2019; accepted 21 April 2020;
https://doi.org/10.1016/j.ymthe.2020.04.020.

[6]These authors contributed equally to this work.

Correspondence: Joo Youn Oh, Department of Ophthalmology, Seoul National University College of Medicine, 103 Daehak-ro, Jongno-gu, Seoul 03080, Korea.
E-mail: bonzoo1@snu.ac.kr
Correspondence: Ryang Hwa Lee, Department of Molecular and Cellular Medicine, Institute for Regenerative Medicine, College of Medicine, Texas A&M University, 1114 TAMU, 206 Olsen Boulevard, College Station, TX 77845, USA.
E-mail: rlee@tamu.edu

MSC-EVs contain a large number of mRNAs, microRNAs (miRNAs), and proteins[19–27] that are responsible for the therapeutic effects of EVs.[28–33] Indeed, treatment of EVs with proteases, RNase, miRNA inhibitors, or small interfering RNAs (siRNAs) for target genes reduced biologic effects of EVs in tissue repair,[28,34] an indication that the effects of MSC-EVs are dependent on proteins and RNAs. However, the molecular mechanism by which MSC-EVs modulate the immune response is not fully understood. In addition, since EVs carry proteins and RNAs of their parent cells, the contents of MSC-EVs would change as their parent MSCs, and therapeutic efficacy of MSC-EVs would largely depend on donors, culture conditions, and tissue sources of MSCs. Hence, identification of a distinctive molecular profile of functionally effective MSC-EVs is crucial to understanding the mechanism underlying the EV-mediated immunomodulation and developing EV-based therapies.

MSCs lose many of their biological properties as they expand beyond about 20 population doublings (PDs) in culture.[35,36] In addition, 3D culture is more beneficial for tissue repair potency of MSCs than conventional monolayer 2D culture because it promotes the self-renewal, differentiation potential, engraftment, homing, and paracrine factor production in MSCs.[37] These data suggest that EVs derived from early-passage MSCs may have better therapeutic potency than do EVs from late-passage MSCs and that EVs from MSCs in 3D culture (3D MSC-EVs) may be more effective than 2D MSC-EVs. Hence, the comparison of molecular profiles between functionally effective EVs and inert EVs would help narrow down a list of candidate therapeutic molecules among numerous factors that EVs contain. Based on these findings, in this study, we purified EVs from early- and late-passage MSCs and from 2D and 3D cultures of MSCs. Then, we compared the immunomodulatory effects between early- and late-passage MSC-EVs and between 2D and 3D MSC-EVs. To evaluate the immunomodulatory effects *in vitro*, we used the following two splenocyte culture systems: T cell receptor (TCR)-mediated activation of resting T cells by anti-CD3 antibodies[38] or anti-CD3/CD28 beads,[39] and Toll-like receptor 4 (TLR4)-mediated activation of splenocytes by lipopolysaccharide (LPS).[40] The immunomodulatory effects of MSC-EVs were further confirmed *in vivo* in mice with systemic LPS challenge and in a mouse model for ocular Sjögren's syndrome, which is a chronic autoimmune disorder characterized by immune cell infiltration and progressive injury to lacrimal glands, leading to keratoconjunctivitis sicca (dry eye disease).[41,42] Since the pathogenesis of ocular Sjögren's syndrome involves activation of Th1 and Th17 cells preceded by activation of innate immune cells via TLRs,[42,43] we evaluated the effects of MSC-EVs on adaptive T cell immunity in lacrimal glands in mice with ocular Sjögren's syndrome,[44] and also examined the effects on TLR4-stimulated innate immunity in mice with systemic LPS administration. Next, to search for therapeutic factors mediating the immunomodulatory effects of MSC-EVs, we compared molecular profiles between functionally effective and ineffective EVs by proteomics and miRNA sequencing and identified the enriched factors in functional EVs. The candidate therapeutic factors in MSC-EVs were verified through inhibition and overexpression of each molecule in MSC-EVs.

RESULTS

Comparison of Immunomodulatory Effects between EVs and Proteins Secreted from MSCs

In this study, we capitalized on a size exclusion chromatography (SEC) method to separate EVs from the conditioned media of MSC cultures and to exclude abundant proteins. After fractionation by SEC, the fractions containing EVs were identified by the EV marker CD63, and the concentration of proteins was measured by Bradford assay. As a result, EVs were enriched in early fractions (see "A" fraction in Figure 1A), whereas most of soluble proteins were eluted in later fractions (see "B" fraction in Figure 1A). The purified EVs were further analyzed for size and EV marker expression. The average size of the purified EV fractions was approximately 100 nm (Figure S1A). As expected, the EV markers CD63, CD81, and CD9 were detected in the purified EV fractions ("A"), but not in the protein fractions ("B") (Figure S1B). Also, EVs maintained their size and spherical structure after storage at −80°C (Figures S1C and S1D).

Both purified EVs and soluble proteins were effective at suppressing the TCR-mediated IL-2 and interferon (IFN)-γ secretion in anti-CD3-stimulated T cells and TLR4-mediated IFN-γ and IL-6 secretion in LPS-stimulated splenocytes (Figures 1B and 1C). However, EVs were more effective at suppressing the production of Th1 and Th17 cytokines, and relatively higher concentrations of the protein were required to achieve the similar suppressive effects to EVs.

To verify the immunomodulatory effect of MSC-EVs *in vivo*, we directly injected the purified EVs or soluble proteins into the intraorbital lacrimal gland in 12-week-old NOD.B10.H2^{b} mice exhibiting a phenotype of ocular Sjögren's syndrome (Figure 1D). One week later, observation of the corneal surface after lissamine green vital staining showed that MSC-EVs markedly improved the epithelial integrity (Figure 1E). The severity of corneal epithelial defects was significantly lower in MSC-EV-treated mice than in PBS- or protein-treated mice (Figure 1F). Similarly, the amount of tear production was increased by MSC-EVs as assessed by a phenol red thread test (Figure 1G). The mRNA levels of inflammatory cytokines tumor necrosis factor (TNF)-α, IL-1β, and IFN-γ were significantly lower in the ocular surface (cornea and conjunctiva) and intraorbital lacrimal gland of MSC-EV-treated mice compared to protein-treated or PBS-treated mice (Figure 1H). Upon periodic acid-Schiff (PAS) staining, the number of conjunctival goblet cells (mucin-secreting cells) was increased by MSC-EVs but not by proteins (Figure 1I). Also, infiltration of T cells in the intraorbital lacrimal gland was significantly attenuated in the MSC-EV-treated group, compared to the protein- and PBS-treated groups (Figure 1J).

Taken together, the data demonstrate that SEC efficiently separates EVs from proteins in the MSC supernatant and that the purified EVs by SEC exhibit better immunosuppressive potency than do the soluble proteins.

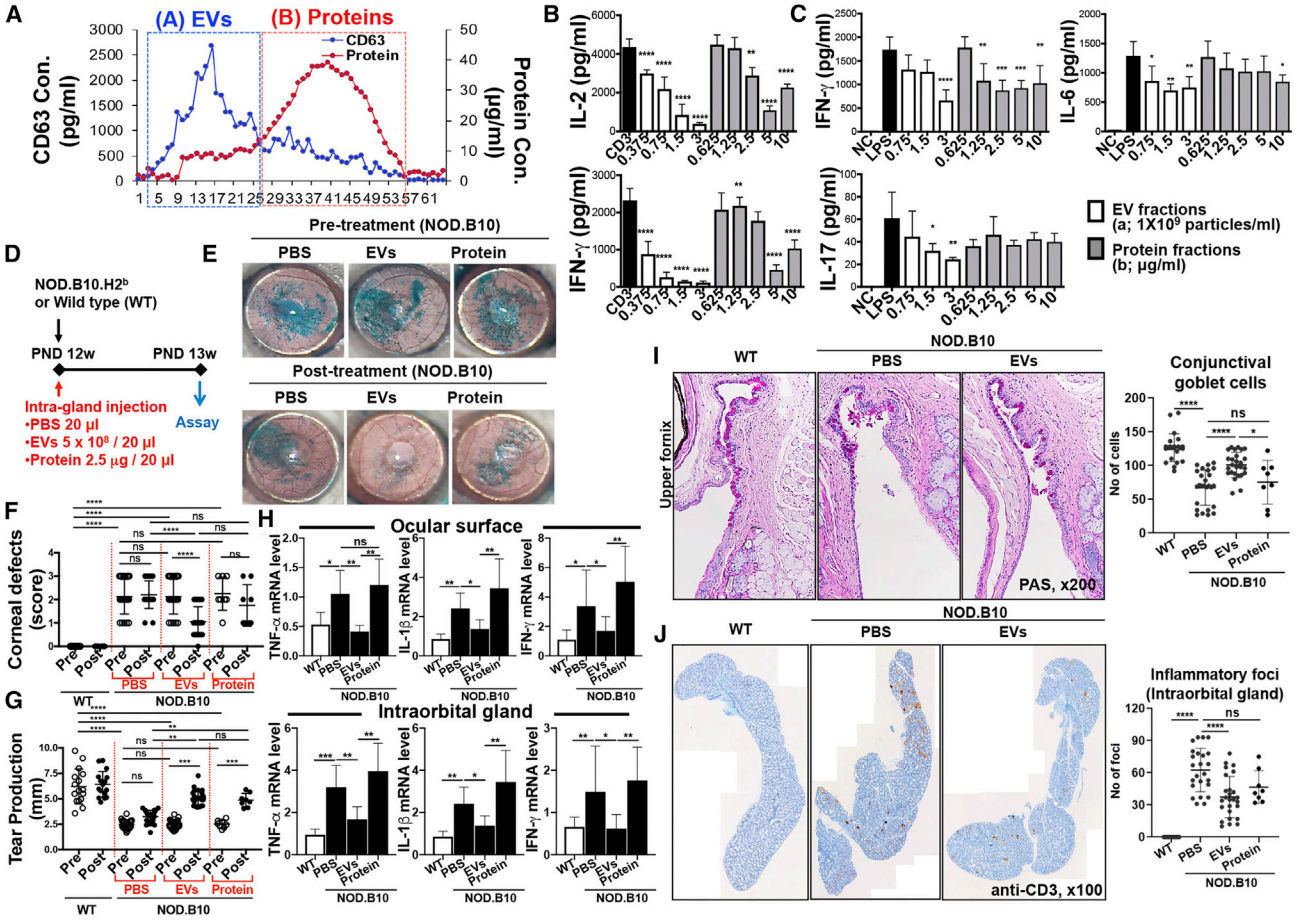

Figure 1. Comparison of EVs versus Proteins Derived from MSCs

(A) Size exclusion chromatography (SEC) elution profile. (B) IL-2 and IFN-γ ELISAs with conditioned medium of splenocytes activated by plate-bound anti-CD3 for 18 h with EVs ("A" fraction) or protein ("B" fraction) in (A) (n = 4). (C) IFN-γ, IL-6, and IL-17 ELISAs with conditioned medium of LPS (50 ng/mL)-stimulated splenocytes for 24 h with or without EVs ("A" fraction) or protein ("B" fraction) in (A) (n = 4). (D) Experimental scheme. (E) Representative ocular surface photographs after lissamine green vital dye instillation. The green-stained area depicts the corneal epithelial defects. (F) Quantitation of corneal epithelial defects before and after treatment. (G) The amount of tear production as determined by a phenol red thread test. (H) Real-time RT-PCR assays for inflammatory cytokines in the ocular surface (containing the cornea and conjunctiva) and intraorbital lacrimal gland. The mRNA levels are presented as the fold expression relative to a normal control wild-type (WT) mouse. (I) Representative PAS staining of conjunctival fornix for visualization of mucin-secreting conjunctival goblet cells (original magnification, ×200) and quantitation of goblet cell counts per eye in each group. (J) Representative CD3 staining of intraorbital lacrimal glands (original magnification, ×100). The number of CD3-stained inflammatory foci per gland was counted and compared between the groups. All data are presented as means ± SD. A dot indicates data from an individual animal. *$p < 0.05$, **$p < 0.01$, ***$p < 0.001$, ****$p < 0.0001$ by one-way ANOVA followed by Dunnett's or Tukey's test. ns, not significant.

Comparison of Immunomodulatory Effects between Early- and Late-Passage MSC-EVs

Next, we compared EVs isolated from early-passage MSCs (about 15 PD levels [PD15][45]) and late-passage MSCs (about 40 PD levels [PD40]). Although the average size and number of the purified EV fractions were similar between PD15 EVs and PD40 EVs (Figures 2A–2C), PD15 MSC-EVs were more effective than PD40 EVs in suppressing the secretion of Th1 and Th17 cytokines in anti-CD3 or anti-CD3/CD28-stimulated splenocytes (Figures 2D and 2E) and IFN-γ secretion in LPS-stimulated splenocytes (Figure 2F). PD40 EVs exhibited similar suppressive effects on the secretion of TNF-α and IL-6 in LPS-stimulated splenocytes compared to PD15 EVs (Figure 2F). These differences in the immunomodulatory efficacies of EVs between early- and late-passage MSCs were also confirmed with MSC-EVs derived from additional donors (Figure 2G).

We went on to compare the effects of PD15 and PD40 MSC-EVs in two animal models. First, we intravenously injected either PD15 or PD40 MSC-EVs in LPS-challenged mice and 5 h later we measured the IL-6 mRNA level in the spleen. Data showed that PD15 MSC-EVs inhibited the level of IL-6 as effectively as dexamethasone (Dex), whereas PD40 EVs partially decreased the IL-6 level (Figure 2H). Second, we injected PD15 or PD40 MSC-EVs into the intraorbital lacrimal gland of 12-week-old

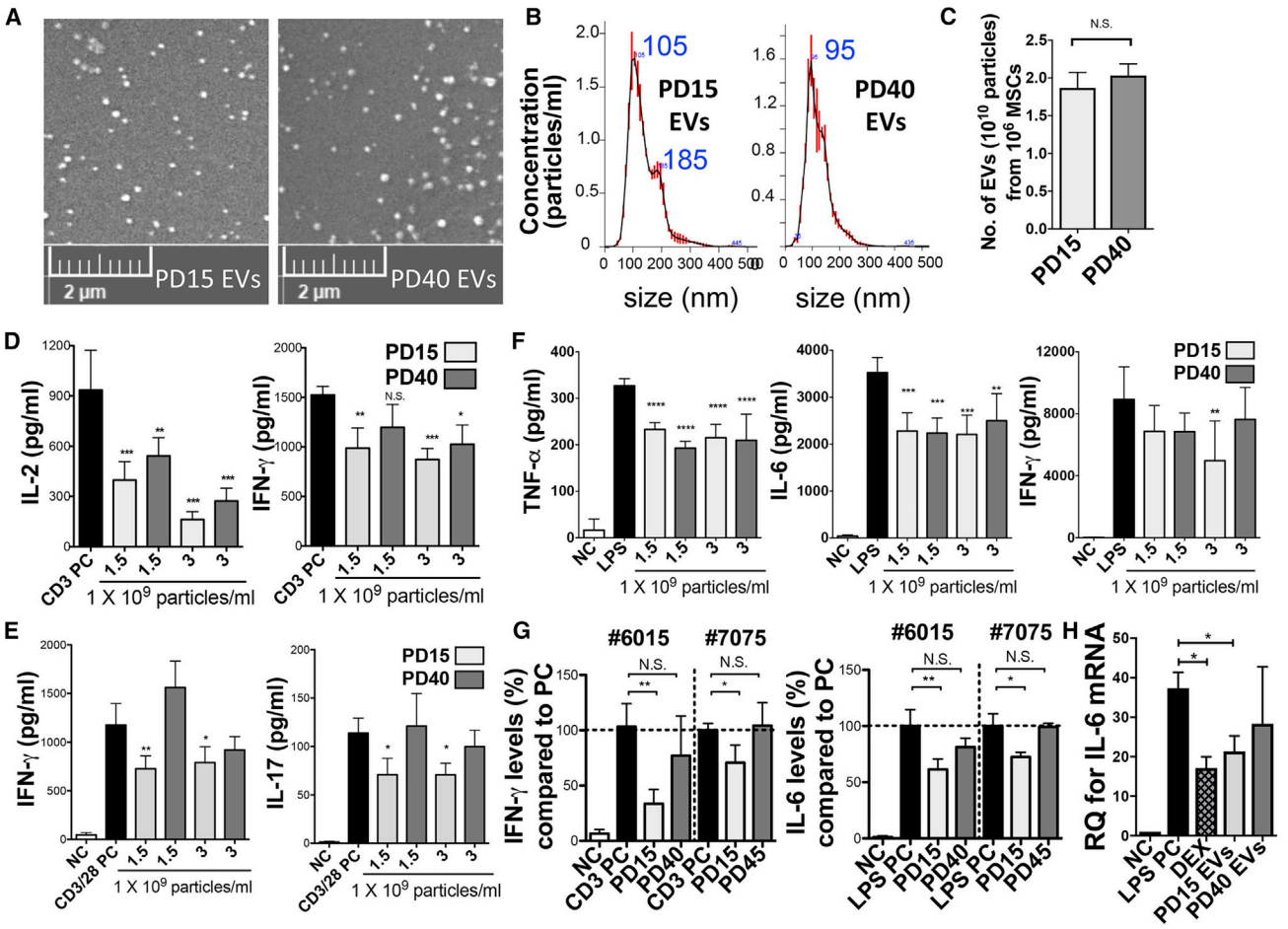

Figure 2. Comparison of the Effect of EVs Derived from Early-Passage MSCs versus Late-Passage MSCs

(A) Representative scanning electron microscopy (SEM) images of PD15 and P40 MSC-EVs. (B) PD15 and PD40 MSC-EV particle sizes by nanoparticle tracking analysis. (C) PD15 and PD40 MSC-EV particle numbers normalized by cell number. (D) IL-2 and IFN-γ ELISAs with conditioned medium of splenocytes activated by plate-bound anti-CD3 for 24 h with or without EVs from PD15 or PD40 MSCs. (E) IFN-γ and IL-17 ELISAs with conditioned medium of anti-CD3/28-stimulated splenocytes for 72 h with or without PD15 or PD40 MSC-EVs. (F) TNF-α, IL-6, and IFN-γ ELISAs with conditioned medium of LPS (50 ng/ml)-stimulated splenocytes for 24 h with or without EVs from PD15 or PD40 MSCs. (G) IFN-γ ELISA with conditioned medium of splenocytes activated by plate-bound anti-CD3 for 24 h with or without EVs (3×10^9/mL) from early- or late-passage MSCs (#7075 and #6015). IL-6 ELISAs with conditioned medium of splenocytes stimulated with LPS (50 ng/mL) for 24 h with or without EVs (3×10^9/mL) from early- or late-passage MSCs (#6015 and #7075) are shown. (H) RT-PCR assay for spleen IL-6 mRNAs at 5 h after intravenous (i.v.) injection of EVs (1×10^{10} particles/mouse) in LPS-challenged mice (30 μg/mouse; i.v.; n = 5/group). EVs were isolated from PD15 or PD40 MSCs. As controls, PBS and DEX (1.5 mg/kg) were injected. Data are presented as means ± SD (n = 4).; *p < 0.05, **p < 0.01, ***p < 0.001, ****p < 0.0001 by one-way ANOVA with Dunnett's test.

NOD.B10.H2^b mice (Figure 3A) and performed assays 1 week later. Both PD15 and PD40 MSC-EVs markedly improved the corneal epithelial integrity and tear production (Figures 3B–3D). However, PD15 EVs were more effective in decreasing corneal epithelial defects and promoting tear production than PD40 EVs (Figures 3B–3D). The levels of pro-inflammatory cytokines were significantly decreased in the ocular surface by PD15 EVs but not by PD40 EVs or PBS (Figure 3E). The conjunctival goblet cell counts were significantly increased by PD15 MSC-EVs but not by PBS or PD40 EVs (Figures 3F and 3G). Also, the infiltration of T cells in the gland was markedly reduced by PD15 EVs, while PD40 EVs did not suppress T cell infiltration (Figures 3H and 3I). These data collectively demonstrate that the EVs purified by SEC exhibit immunosuppressive potency *in vitro* as well as in LPS-challenged mice, and they protect the ocular surface and lacrimal gland against inflammatory damage in mice with ocular Sjögren's syndrome. Both early- and late-passage MSC-EVs are effective, but the immunomodulatory effects are higher with EVs from early-passage MSCs than those from late-passage MSCs.

Protein Profiles of MSC-EVs

In order to identify a distinctive protein profile of functionally effective EVs in immunomodulation, we compared protein expression profiles between PD15 and PD40 MSC-EVs. As in Figures 2

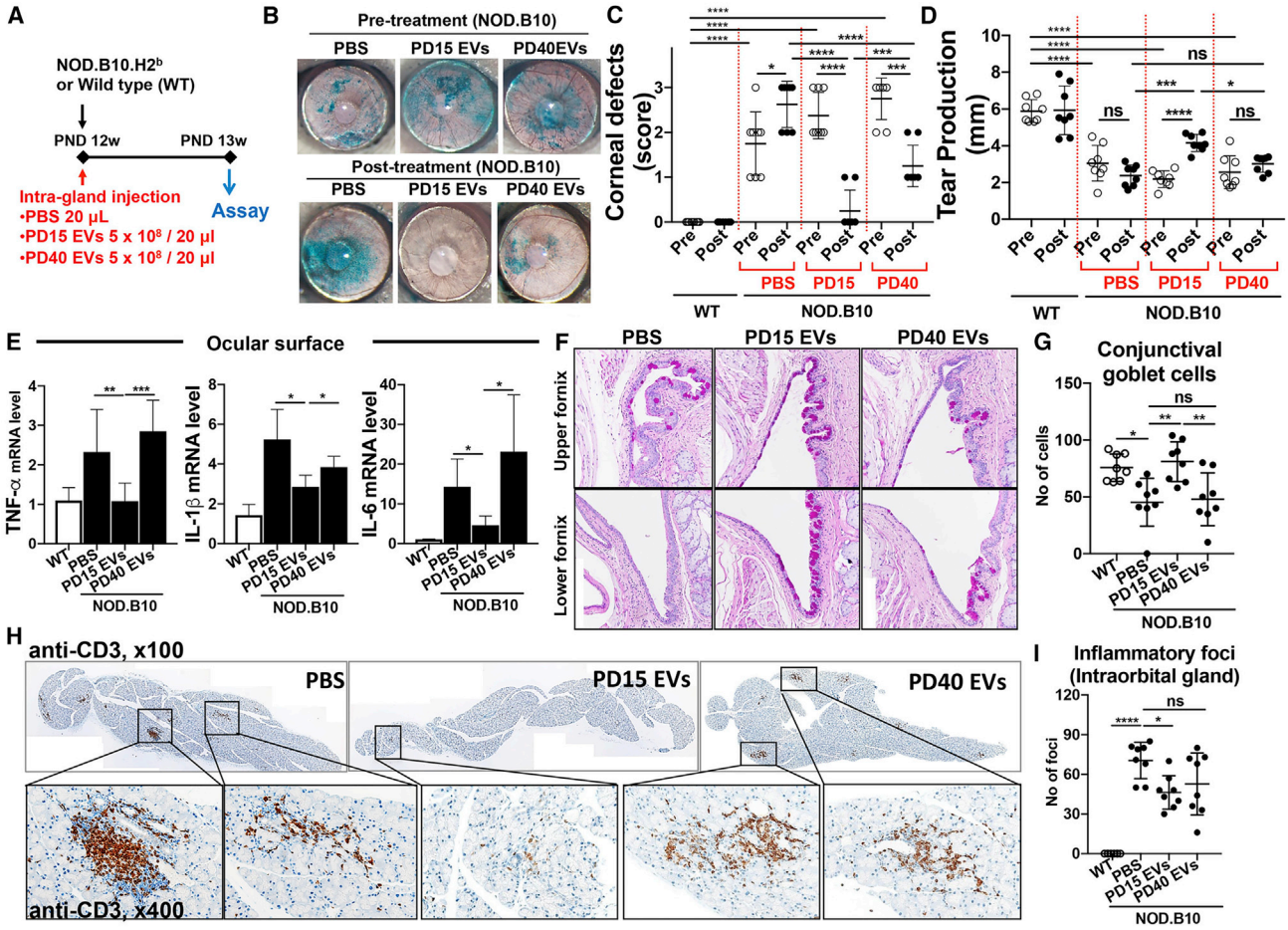

Figure 3. Comparison of Immunomodulatory Effects of EVs from Early- versus Late-Passage MSCs in a Mouse Model of Ocular Sjögren's Syndrome

(A) Experimental scheme. (B) Ocular surface photograph after lissamine green staining to visualize the area of corneal epithelial defect. (C and D) The quantitation of corneal epithelial defects (C) and aqueous tear production (D) before and after treatment. (E) mRNA levels of inflammation-related cytokines in the ocular surface as measured by real-time RT-PCR. Shown are the values relative to normal wild-type (WT) mice. (F and G) PAS staining of the conjunctival fornix (F) to determine conjunctival goblet cells (original magnification, ×200) and the number of goblet cells per eye (G). (H) CD3 staining of the intraorbital lacrimal gland. (I) The number of CD3-stained foci per gland is presented. All data are presented as means ± SD. A dot represents data from an individual animal. *p < 0.05, **p < 0.01, ***p < 0.001, ****p < 0.0001 by one-way ANOVA followed by Tukey's test. ns, not significant.

and 3, PD40 MSC-EVs were less effective in suppressing immune responses, an indication that downregulated factors in PD40 MSC-EVs compared to PD15 EVs could be related to the loss of their immunosuppressive functions and that enriched factors in PD40 EVs might interfere with the effects of MSC-EVs. Therefore, enriched factors (at least 2-fold) in PD15 and PD40 MSC-EVs (Figure 4A) were analyzed using Protein Analysis through Evolutionary Relationships (PANTHER) software.[46] When the proteins enriched in PD15 or PD40 EVs were classified according to molecular function, catalytic activity, binding, and structural molecule activity, binding was the most common molecular function of the differentially expressed proteins (Figure 4B). The proteins classified as binding were further analyzed according to protein class. As a result, most of the PD15 EV proteins were classified as protein-binding proteins. In contrast, more than 50% of the PD40 EV-binding proteins were classified as nucleotide/nucleic acid binding (Figure 4C).

Then, we validated the differential expression levels of the top-ranked binding proteins in PD15 EVs in Figure 4D. Especially, we tested whether these proteins are expressed on the surface of EVs or inside of EVs utilizing ELISA with or without lysis (Figure 4E). Consistent with proteomics, the results showed that TGFβI (TGF-beta-induced protein), PTX3 (pentraxin 3), EDIL3 (EGF-like repeat and discoidin I-like domain-containing protein 3), BGN (biglycan), LUM (lumican), and GAL3 (galectin-3) were highly expressed in PD15 EVs compared to the PD40 EVs (Figure 4F). In addition, when EVs were treated with lysis buffer, the levels of EDIL3 and BGN were significantly increased in EVs (Figure 4F), indicating that these proteins were located on the EV membrane as well as within EVs.

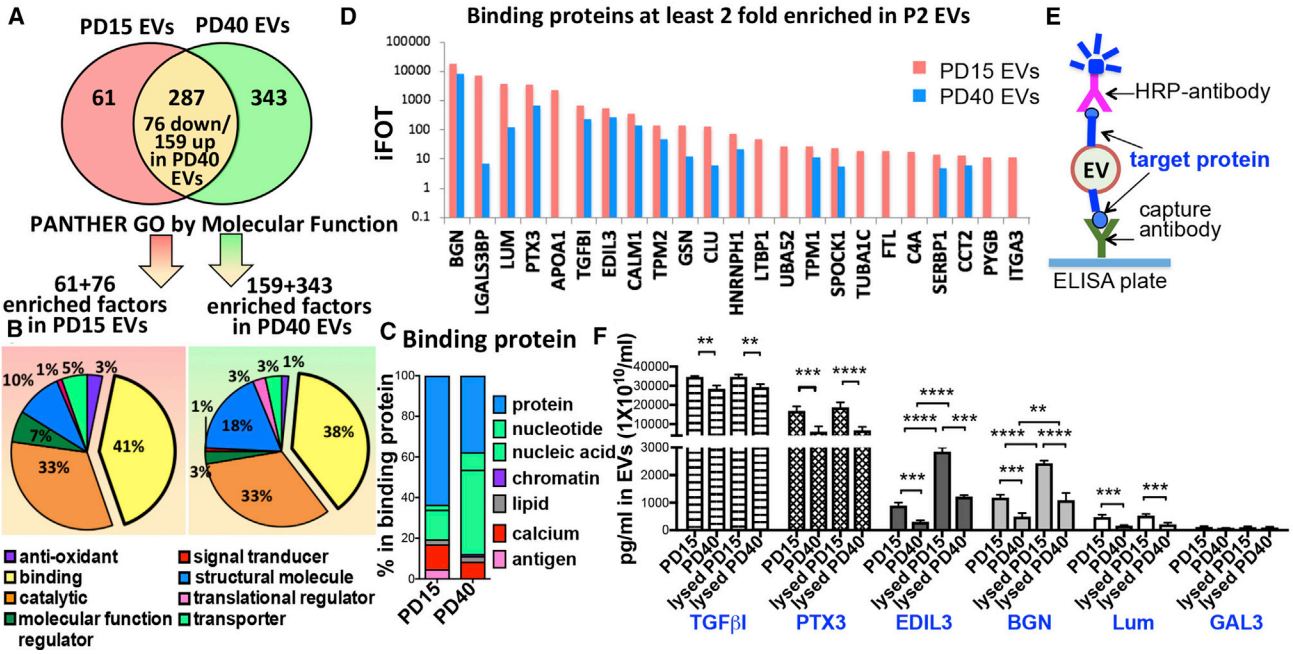

Figure 4. Protein Profiles of EVs from Early-Passage MSCs and Late-Passage MSCs

(A) Venn diagram of protein profiling of PD15 and PD40 MSC-EVs. (B) Classification of proteins enriched in PD15 or PD40 EVs according to molecular function. (C) Distribution of binding protein composition of PD15 and PD40 MSC-EVs. (D) Top ranked binding proteins at least 2-fold enriched in PD15 MSC-EVs. (E) Schematic of the ELISA in (F) to measure the concentration of target protein on the surface of EVs. (F) ELISAs of proteins in PD15 and PD40 MSC-EVs with or without lysis buffer treatment (n = 3; three different preparations). Data are presented as means ± SD. **p < 0.01, ***p < 0.001, ****p < 0.0001 by one-way ANOVA with Tukey's test.

Therefore, the proteomics data reveal that early- and late-passage MSC-EVs have different protein profiles, and extracellular region or matrix proteins TGFβI, PTX3, EDIL, BGN and LUM are enriched in early-passage MSC-EVs while nucleic-acid binding proteins are enriched in late-passage MSC-EVs.

Comparison of Immunomodulatory Effects and Protein Profiles between EVs Derived from MSCs Expanded under a 2D and 3D Culture System

We next tested whether a 3D culture system (Figure 5A) might promote the immunosuppressive effects of MSC-EVs, as previous reports showed the superior therapeutic effects of 3D-cultured MSCs to 2D-cultured MSCs.[37] EVs were isolated from PD15 MSCs that had been expanded under a 2D or 3D culture system, and the immunomodulatory functions of EVs were measured in *in vitro* and *in vivo* assays. Results showed that EVs derived from 3D MSCs more effectively suppressed the secretion of pro-inflammatory cytokines IFN-γ and IL-6 and induced the production of immunoregulatory cytokines TGF-β1 and IL-10 in anti-CD3/CD28-stimulated splenocytes (Figure 5B). Consistent with these *in vitro* results, the serum levels of TNF-α, IL-6, and IL-17 were significantly reduced in LPS-challenged mice after treatment with MSC-EVs, and 3D MSC-EVs were more effective than 2D MSC-EVs (Figure 5C).

In order to identify upregulated factors in 3D MSC-EVs, we performed proteomics in EVs isolated from PD15 MSCs expanded under a 2D or 3D culture system. As a result, proteomics identified about 600 proteins in the MSC-EVs. Among them, 186 proteins were found in both 2D and 3D MSC-EVs, with 97 proteins being upregulated in 3D MSC-EVs (Figure 5D). When the upregulated proteins in 3D EVs were classified according to molecular function, the most common functions of the enriched proteins were binding and catalytic activity (Figure 5E). Among the binding proteins, about 25% of them were classified as a signaling molecule, most of which were TGF-β signaling-related genes: TGF-β1, TGF-β2, and TGFβI (Figure 5F). According to the biological process, the enriched proteins in 3D EVs (Figure 5G, >1.5-fold enriched factors in 3D EVs; Figure 5H, proteins found only in 3D EVs) were predominantly involved in the cellular process, stimulus, and biological adhesion. Of them, TGF-β signaling-related genes, i.e., TGF-β1, TGF-β2 and TGFβI, were markedly upregulated in 3D MSC-EVs compared to 2D MSC-EVs. In addition, TSG-6 was highly increased in 3D MSC-EVs whereas 2D EVs contained a low level of TSG-6, which is consistent with our previous observation that TSG-6 is secreted by MSCs upon inflammatory cytokine stimulation or under 3D culture system.[47,48] Therefore, we confirmed the differential expression levels of TGF-β1, TGF-β2, TGFβI, and TSG-6 in 3D MSCs versus 2D MSCs as well as in 3D MSC-EVs versus 2D EVs (Figure 5I). Additionally, we found that the level of TGF-β1 was slightly increased in EVs when the EVs were treated with lysis buffer, and the membrane-bound TGF-β1 was significantly downregulated in PD40 EVs compared to PD15 EVs (Figure 5J).

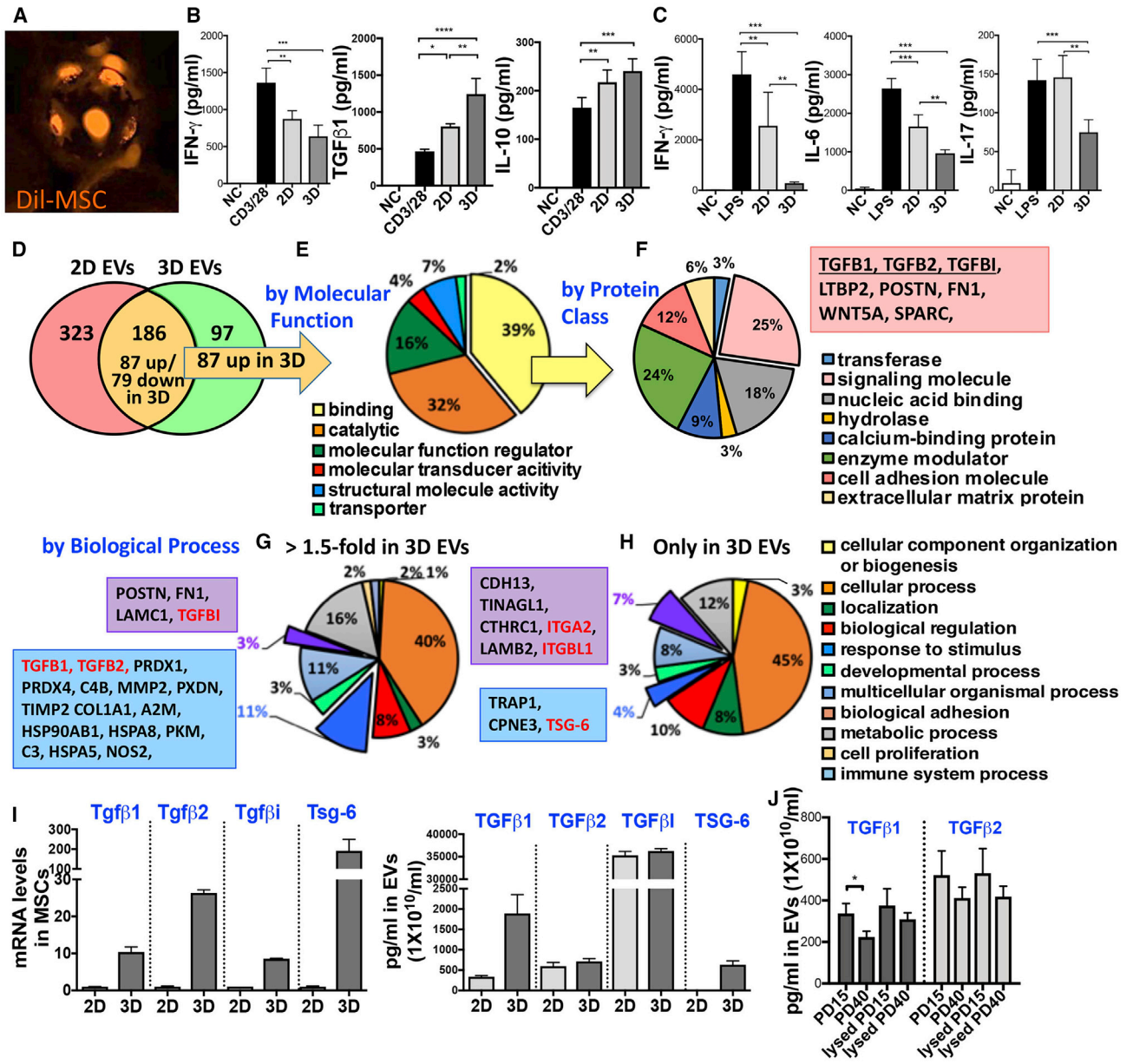

Figure 5. Comparison of the Immunomodulatory Effect and Protein Profiles between EVs Derived from MSCs Expanded under 2D versus 3D Culture System

(A) Representative photograph of fluorescence (DiI)-labeled MSCs on microcarriers (Corning Life Sciences) at 4 h after seeding. (B) IFN-γ, IL-6, TGF-β1, and IL-10 ELISA with conditioned medium of anti-CD3/28-stimulated splenocytes for 72 h with or without 2D or 3D MSC-EVs (1.5×10^9 particles/mL; n = 4). (C) ELISA for serum cytokines (TNF-α, IL-6, and IL-17) at 5 h after EV injection (1×10^{10} particles/mouse) in LPS-challenged mice (30 μg/mouse; i.v.; n = 5/group). EVs were isolated from PD15 MSCs expanded in 2D culture (CellStack cell culture chambers; Corning Life Sciences) or 3D culture (microcarriers in a spinner flask; Corning Life Sciences). All data are presented as means ± SD. *$p < 0.05$, **$p < 0.01$, ***$p < 0.001$ by one-way ANOVA with Tukey's test. (D) Venn diagram of protein profiling of 2D and 3D MSC-EVs. (E) Classification of proteins found in both, but enriched (1.5-fold) in 3D MSC-EVs compared to 2D according to molecular function. (F) Classification of binding proteins in (E). (G) Classification of proteins found in both, but enriched (1.5-fold) in 3D MSC-EVs compared to 2D according to biological process. (H) Classification of proteins found only in 3D MSC-EVs according to biological process. (I) RT-PCR assays for TGF-β1, TGF-β2, TGFβI, and TSG-6 mRNA in 2D and 3D MSCs and ELISAs for TGF-β1, TGF-β2, TGFβI, and TSG-6 protein in 2D and 3D MSC-EVs (n = 3; three different preparations). (J) ELISAs of TGF-β1 and TGF-β2 proteins in PD15 and PD40 MSC-EVs with or without lysis buffer treatment (n = 3; three different preparations). All data are presented as means ± SD. *$p < 0.05$ by one-way ANOVA with Tukey's test.

Hence, the results support the notion that the contents of EVs change as their parent cells change. Additionally, our comparative analysis with proteomics revealed that TGF-β1, TGF-β2, and TGFβI are upregulated in 3D MSC-EVs compared to 2D MSC-EVs, and TGF-β1 and TGFβI are downregulated in late-passage (PD40) 2D MSC-EVs.

Identification of Therapeutic Factors Responsible for Immunomodulatory Effects of MSC-EVs

To examine whether the upregulated proteins in early-passage MSC-EVs are responsible for the EV-mediated effect in ocular Sjögren's syndrome (Figure 3), we first screened for the effects of an individual recombinant human protein in cultures of mouse splenocytes. Considering the expression levels of putative candidates for therapeutic proteins in EVs (Figures 4F and 5I), we adopted higher levels of PTX3, TGFβI, LUM, and EDIL3 than TGF-β1 and TGF-β2 for use in assays. As expected, recombinant human (rh)TGF-β1 was most effective in inhibiting IFN-γ secretion in anti-CD3/CD28-stimulated splenocytes, even at as low a concentration as 2.5 ng/mL (Figure 6A). The rhTGF-β2 was also effective but required a higher concentration than rhTGF-β1 (Figure 6A). Of the tested proteins, rhPTX3, rhTGFβI, and rhLUM were also effective (Figure 6A). Therefore, we selected TGF-β1, TGFβI, PTX3, and LUM as candidate molecules mediating the therapeutic effects of MSC-EVs and validated the role of these proteins in ocular Sjögren's syndrome. In order to inhibit the expression of TGF-β1, TGFβI, PTX3, or LUM in MSC-EVs, we downregulated the expression of these target genes in PD15 MSCs with siRNAs (Figure S2A). Manipulation of MSCs with siRNAs successfully decreased the target protein levels in their EVs (Figure 6B). Notably, silencing the individual gene in MSCs, except LUM, decreased not only its target protein level in their EVs but also the expression of other candidates in EVs. For example, silencing TGF-β1 in MSCs affected the level of TGFβI in EVs as well as the TGF-β1 level (Figure 6B), which is expected because TGFβI is induced by TGF-β1. Analogously, silencing PTX3 in MSCs partially decreased the expression of all other candidates in their EVs (Figure 6B).

Next, we investigated the suppressive effects of the manipulated EVs in splenocyte cultures and in NOD.B10.H2^b mice. Silencing TGF-β1 or PTX3 in MSCs most significantly abrogated the suppressive effects of their EVs (Figures 6C–6F). The EVs lacking PTX3 or TGF-β1 were less effective in attenuating corneal epithelial defects and preserving tear production and goblet cells in NOD.B10.H2^b mice than were control EVs or EVs lacking LUM (Figures 6D–6F). In contrast, when we overexpressed TGF-β1 or PTX3 in EVs by transfection of cDNA plasmids in PD15 MSCs (Figures S2B and S2C), the EVs became more effective, and even lower doses of EVs were sufficient to suppress TCR downstream IL-2 (Figure S2D) and IFN-γ secretion (Figure 6G) in splenocytes activated by anti-CD3. Also, they more effectively suppressed IL-6 and IL-17 production in TLR4-stimulated splenocytes (Figure 6H; Figure S2E). Therefore, these results clearly demonstrate that TGF-β1 and PTX3 are major therapeutic factors responsible for the EV-mediated TCR and TLR4 suppression. These differential expression patterns of TGF-β1 and PTX3 were further confirmed in the conditioned medium of early-passage and late-passage MSCs (Figure S2F) and in early- and late-passage MSC-EVs derived from two additional donors (Figure S2G).

Since TCR and TLR4 downstream genes were more highly suppressed by EVs overexpressing TGF-β1 or PTX3, we examined the molecular mechanism by which MSC-EVs suppress the activation of splenocytes. Activation of T cells by antigens or cytokines leads to nuclear translocation of nuclear factor κB (NF-κB), activator protein 1 (AP-1), nuclear factor of activated T cells (NFAT), and signal transducer and activator of transcription (STAT) transcription factors and thereby induces the expression of genes that are important for growth, differentiation, and cell adhesion.[49,50] In fact, after 3 h of MSC-EV treatment, we found a reduction in nuclear translocation of the transcription factors NF-κB and NFAT1 in stimulated splenocytes (Figure 6I; Figure S2H), reflecting the suppression of TCR signaling by MSC-EVs. Furthermore, MSC-EVs directly suppressed phosphorylation of LAT (linker for activation of T cells) (Figure 6j), which is associated with critical proteins, including enzymes and adapters that regulate most TCR-dependent responses.[51] Activation of TLR4 by LPS induces nuclear translocation of NF-κB and p38 mitogen-activated protein kinases (MAPK) and increases the inflammatory cytokines, including TNF-α and IL-6.[52,53] After 1 h of treatment, we also found a reduction in nuclear translocation of the transcription factors NF-κB and p38 in stimulated splenocytes by MSC-EVs (Figure 6K; Figure S2I).

These results collectively demonstrate that MSC-EVs directly suppress the TCR and TLR4 downstream genes and that TGF-β1 and PTX3 are major therapeutic factors responsible for the EV-mediated TCR and TLR4 suppression.

miRNA Profiles of MSC-EVs

To identify a miRNA profile of functionally effective EVs in immunomodulation, we carried out miRNA sequencing with PD15 EVs, PD40 EVs, and 3D EVs. A Venn diagram shows the number of miRNAs expressed in all EVs (Figure 7A). As miRNAs directly regulate signal transduction and EVs from late passage MSCs were also effective in mice with ocular Sjögren's syndrome, we focused on the top 10 ranked miRNAs found in PD15 EVs among 180 miRNAs that were commonly expressed in all three EV groups. The top 10 ranked miRNAs in PD15 EVs were expressed at similar levels to 3D EVs and PD40 EVs, but let-7b-5p was increased in 3D MSC EVs while miR-21-5p was decreased (Figure 7B). The volcano plots based on p values and fold changes of the differentially expressed miRNAs showed that there was a huge change between 2D EVs and 3D EVs, but miRNAs of PD40 EVs were mostly downregulated compared to 2D EVs (Figure 7C). Also, let-7b-5p was the most significantly upregulated miRNA in 3D EVs and downregulated in PD40 EVs, and miR-21-5p, the most enriched miRNA in 2D EVs, was downregulated in 3D EVs (Figure 7C). To fully inspect the function of the top two miRNAs, let-7b-5p and miR-21-5p, we analyzed KEGG (Kyoto Encyclopedia of Genes and Genomes) pathway annotation of the predicted miRNA targets using the miRSystem web server (http://mirsystem.cgm.ntu.edu.tw). The result shows that they are involved in multiple pathways,

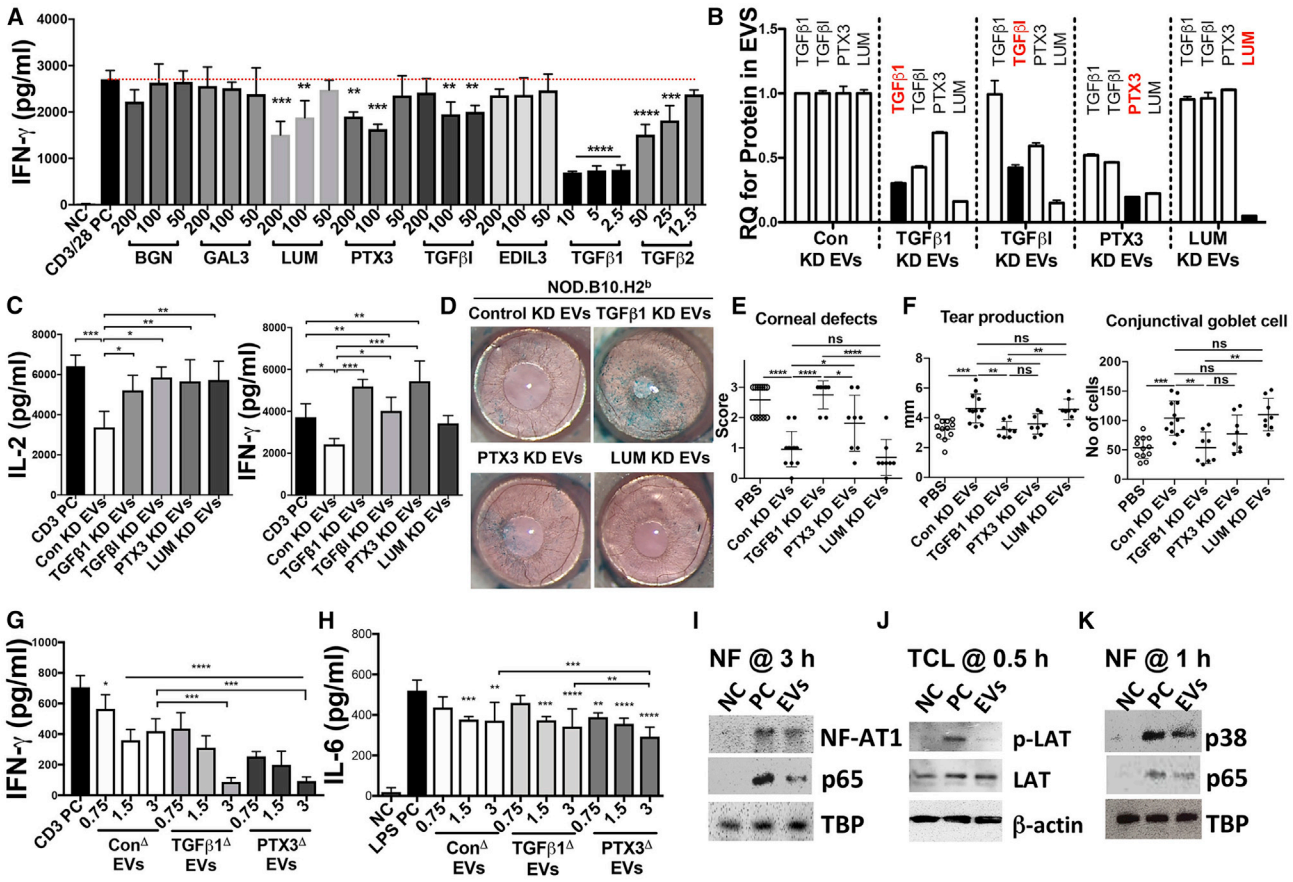

Figure 6. Immunomodulatory Effects of EVs from MSCs with Manipulation of TGF-β1 and PTX3 Expression

(A) IFN-γ ELISA with conditioned medium of anti-CD3/28-stimulated splenocytes for 72 h with or without recombinant human (rh) proteins (0–200 ng/mL) (n = 4). (B) ELISAs for protein levels of TGF-β1, TGFβI, PTX3, and LUM in MSC-EVs derived from MSCs transfected with target siRNAs. (C) IL-2 and IFN-γ ELISAs with conditioned medium of splenocytes activated by plate-bound anti-CD3 for 24 h with EVs derived from MSCs transfected with target siRNAs (n = 4). (D and E) Ocular surface photography with lissamine green staining (D) and quantitation of corneal epithelial defects using a standardized scoring system (E). (F) Aqueous tear production as quantified by a phenol red thread test and numeration of conjunctival goblet cells on PAS-stained conjunctival specimens. A dot indicates data from a single animal. (G) IFN-γ ELISA with conditioned medium of splenocytes activated by plate-bound anti-CD3 for 24 h. (H) IL-6 ELISA with conditioned medium of LPS-stimulated splenocytes for 24 h with EVs derived from PD15 MSCs transfected with target DNA plasmids (n = 4). All data are presented as means ± SD. *$p < 0.05$, **$p < 0.01$, ***$p < 0.001$, ****$p < 0.0001$ by one-way ANOVA with Dunnett's or Tukey's test. (I) Western blot assays with nuclear factions (NFs) of anti-CD3/28-stimulated splenocytes for 3 h with or without MSC-EVs (3×10^9 particles/mL). (J) Western blot assays with total cell lysates (TCLs) of anti-CD3/28-stimulated splenocytes for 30 min with or without MSC-EVs (3×10^9 particles/mL). (K) Western blot assays with nuclear factions (NFs) of LPS-stimulated splenocytes for 1 h with or without MSC-EVs (3×10^9 particles/mL).

including MAPK, JAK (Janus kinase)-STAT, TLR, and TCR signaling pathways (Table S1). As such, miR-21-5p and let-7b-5p were selected as the potential miRNA signature for further analysis based on expression levels in EVs, p values, and known target pathways. Consistent with the miRNA sequencing data, we found that let-7b-5p was decreased in PD40 EVs and miR-21-5p was slightly higher in PD40 EVs than in PD15 EVs (Figure 7D). Also, we confirmed that let-7b-5p was significantly decreased in late-passage MSC-EVs with additional donor-derived MSCs and miR-21 was also decreased (Figure S3A). Moreover, the 3D culture system increased let-7b-5p in MSC-EVs while decreasing miR-21-5p in MSC-EVs (Figure 7D). Importantly, silencing let-7b-5p and miR-21-5p in MSCs (Figure S3B) abrogated the inhibitory effects of their EVs on the secretion of IFN-γ, IL-17, and IL-6 in stimulated splenocytes (Figures 7E and 7F) and partially affected the production of the regulatory cytokine TGF-β1 in splenocytes (Figure 7E). Also, inhibition of let-7b-5p decreased the expression level of PTX3 in their EVs (Figure S3C).

Therefore, these data suggest that let-7b-5p and miR-21-5p are responsible for the EV-mediated inhibition in both TCR- and TLR4-signaling downstream genes.

Positive Correlation between TGF-β1, PTX3, let-7b-5p, or miR-21-5p Levels in EVs and Their Immunomodulatory Potency

Another interesting finding we observed is that as the cell density increased, the levels of TGF-β1, PTX3, let-7b-5p, and miR-21-5p

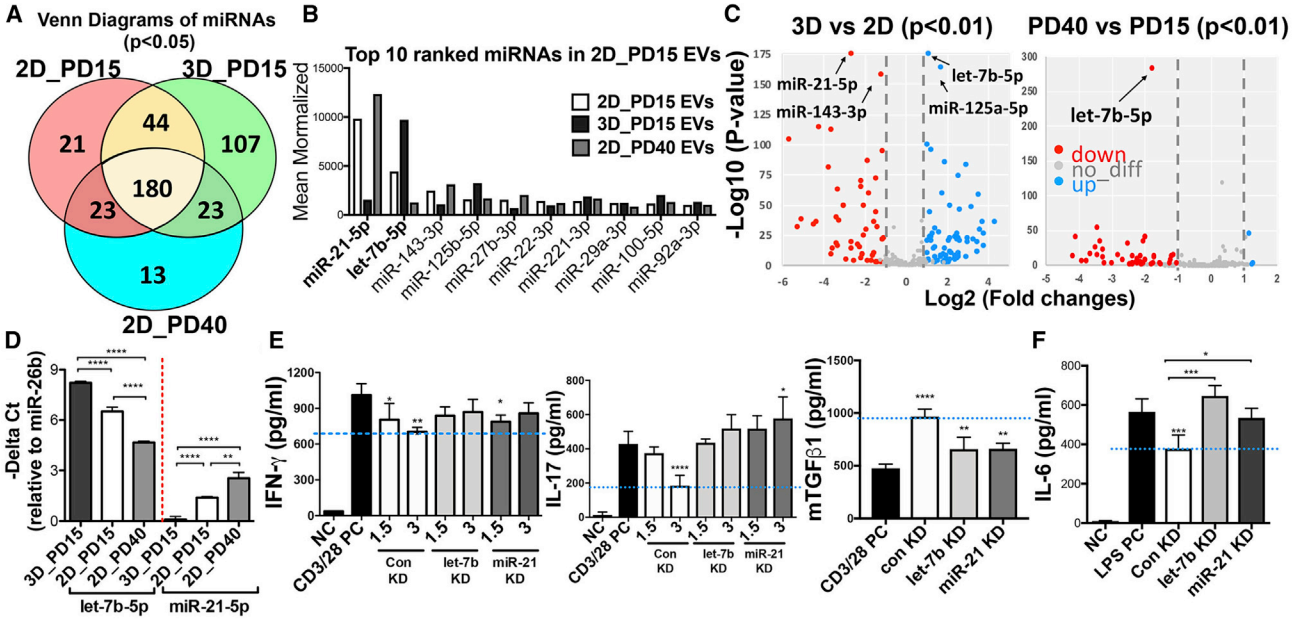

Figure 7. Comparison of miRNA Profiles of EVs from Early-Passage MSCs, 3D MSCs, and Late-Passage MSCs

(A) Venn diagram of miRNAs expressed in 2D_PD15 EVs, 3D_PD15 EVs, and 2D_PD40 EVs. (B) Top 10 ranked miRNAs in 2D_PD15 EVs. (C) Volcano plot of the differentially expressed miRNAs in 2D_PD15 EVs versus 3D EVs or PD40 MSC-EVs. The y axis indicates the −log 10 of the p values and the x axis is the fold change (FC) (measured as the log_2-transformed ratio of the expression between both experimental groups). (D) Confirmation of relative let-7b and miR-21-5p expression in EVs from 2D-cultured PD15 and PD40 MSCs and 3D-cultured PD15 MSCs. (E) IFN-γ, IL-17, and TGF-β1 ELISAs with conditioned medium of anti-CD3/28-stimulated splenocytes for 72 h with or without EVs from PD15 MSCs transfected with target miRNA inhibitor (n = 4). (F) IL-6 ELISA with conditioned medium of LPS-stimulated splenocytes for 24 h with EVs derived from PD15 MSCs transfected with target miRNA inhibitor (n = 4). All data are presented as means ± SD. *p < 0.05, **p < 0.01, ***p < 0.001, ****p < 0.0001 by one-way ANOVA with Dunnett's or Tukey's test.

gradually increased in MSC-EVs (Figures 8A and 8BC). Accordingly, EVs from high-density MSCs (about 80% confluency; ~12,000 cells/cm^2) more effectively suppressed TCR signaling in CD3/CD28-stimulated splenocytes and TLR4 signaling in LPS-stimulated splenocytes (Figure 8C). Notably, a high dose of EVs from low-density MSCs (about 60% confluency; ~3,000 cells/cm^2) had no effect on TCR-stimulated splenocytes and rather increased IL-17 production (Figure 8C) while being still effective at the suppression of TLR4-stimulated splenocyte activation (Figure 8D). Similarly, EVs from late-passage MSCs were still effective in suppressing TLR4 signaling (Figure 2F), although they contained a low level of TGF-β1 (Figure 5J). Therefore, we next analyzed correlations between the expression levels of these factors in EVs isolated from different cell density, different cell passage, and different donors and their inhibitory function on TCR and TLR4 signaling so as to define biomarkers predictive of the regulatory function of EVs. Results showed that the inhibitory function of EVs on TLR4 signaling was more strongly correlated with their PTX3, let-7b, and miR-21 levels, while TGF-β1 levels of MSC-EVs were strongly correlated with their suppressive effects on TCR signaling (Figure 8E). Furthermore, when we overexpressed TGF-β1 or PTX3 in late-passage MSCs, let-7b-5p and miR-21-5p levels were also increased in MSCs (Figure 8F), and their EVs were more effective at the suppression of TCR and TLR4 downstream genes in activated splenocytes (Figure 8G).

Hence, the data suggest that all of the key factors identified in MSC-EVs synergistically contribute to the regulatory function of EVs and thus can be used as signature molecules of functionally effective MSC-EVs.

DISCUSSION

Our data demonstrate that EVs derived from early-passage MSCs suppress Th1 and Th17 cytokines in splenocyte cultures and improve inflammatory dry eye disease in mice with ocular Sjögren's syndrome more effectively than do late-passage MSC-EVs. In addition, the immunomodulatory activities of EVs are enhanced even further when the EVs are produced from MSCs expanded under a 3D culture system. Through the comparative molecular profiling, we found that EVs from early-passage MSCs contain high levels of TGF-β1, PTX3, and let-7b-5p, compared to those from late-passage MSCs and that both EVs from early- and late-passage MSCs contain high levels of miR-21-5p. Importantly, inhibition or overexpression of TGF-β1, PTX3, let-7b-5p, or miR-21-5p in MSCs significantly abrogates or promotes the suppressive effect of their EVs on Th1 and Th17 cytokine production. In addition, TGF-β1, PTX3, let-7b-5p, and miR-21-5p levels in MSC-EVs show a strong positive correlation with their suppressive function. Therefore, our strategy of comparative molecular profiling of MSC-EVs herein reveals TGF-β1, PTX3, let-7b-5p,

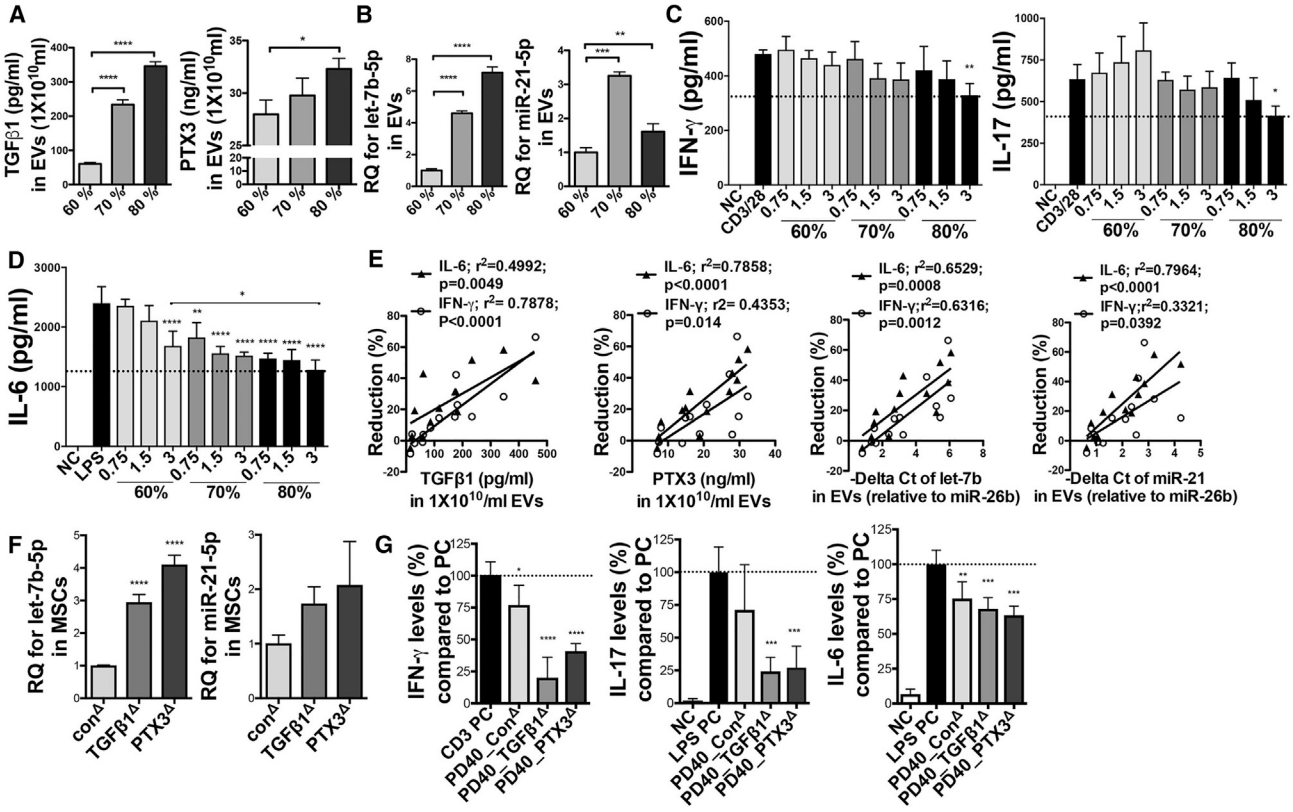

Figure 8. Correlations between TGF-β1, PTX3, let-7b-5p, or miR-21-5p Levels in EVs and Their Inhibitory Effects on TCR and TLR4 Signaling

(A) ELISAs of TGF-β1 and PTX3 in PD15 EVs derived from MSCs with different cell density. (B) Relative expressions of let-7b-5p and miR-21-5p in PD15 EVs derived from MSCs with different cell density. (C and D) IFN-γ and IL-17 with conditioned medium of anti-CD3/28-stimulated splenocytes for 72 h (C), and IL-6 ELISAs with conditioned medium of LPS-stimulated splenocytes for 24 h (D) with or without EVs from MSCs with different cell density. (E) Correlations between the levels of TGF-β1, PTX3, let-7b-5p, or miR-21-5p in PD15 EVs derived from MSCs with different cell density (60%–80%) or in early- or late-passage MSC-EVs from different donors (#6015, and #7075) and their suppressive efficacy on IL-6 or IFN-γ production (reduction % of IL-6 or IFN-γ production compared to the positive control). (F) Relative expressions of let-7b-5p and miR-21-5p in MSCs transfected with target DNA plasmids. (G) IFN-γ ELISA with conditioned medium of splenocytes activated by plate-bound anti-CD3 for 24 h, and IL-6 and IL-17 ELISAs with conditioned medium of LPS-stimulated splenocytes for 24 h with EVs derived from PD40 MSCs transfected with target DNA plasmids (n = 4). All data are presented as means ± SD. *p < 0.05, **p < 0.01, ***p < 0.001, ****p < 0.0001 by one-way ANOVA with Dunnett's or Tukey's test.

and miR-21-5p as key effectors mediating the EV-mediated immunomodulation.

Previously, we reported that MSC-EVs directly suppressed the activation of T cells and APCs, thereby inhibiting the development of Th1 and Th17 cells.[3] In the present study, we further defined the molecular mechanisms underlying the EV-mediated inhibition of Th1 and Th17 cells. Our data showed that MSC-EVs suppressed TLR4 and TCR downstream signaling pathways in activated splenocytes. In particular, MSC-EVs directly suppressed phosphorylation of LAT, a direct downstream of TCR, and subsequent nuclear translocation of NFAT1 and NF-kB. Also, MSC-EVs suppressed nuclear translocation of NF-kB and p38 in TLR4-stimulated splenocytes. In addition, manipulation of TGF-β1 or PTX3 in early-passage MSCs directly affected the inhibitory function of their EVs on the expression of TCR and TLR4 signaling downstream genes. TGF-β1 is a well-known immunoregulatory cytokine that uses distinct signaling mechanisms in immune cells to affect T cell homeostasis and regulatory T cells.[54] Consistent with our observations, a previous study demonstrated that TGF-β1 represses IL-2 production in TCR-activated T cells by inhibiting Tec kinases that increase NFAT translocation.[55] Also, despite the long-debated role of PTX3 in autoimmune disease,[56] a recent study showed that PTX3 knockout mice exhibited enhanced IL-17A levels, and PTX3-deficient dendritic cells increased the production of Th17 polarizing cytokine IL-6 and IL-23.[57] Therefore, previous studies support our findings that TGF-β1 and PTX3 are major therapeutic factors responsible for the EV-mediated inhibition of TCR and TLR4 signaling downstream genes. Furthermore, we showed that inhibition of let-7b-5p and miR-21-5p in MSC-EVs negated the suppressive effect of EVs on the production of Th1/Th17 cytokines and failed to increase the regulatory cytokine TGF-β1 in splenocytes. In line with our observation, recent studies reported that let-7b targets TCR signaling[58,59] and both let-7b and miR-21 modulate macrophage polarization,[60–62] possibly by

targeting the TLR4 signaling pathway.[63–67] On the contrary, there are reports showing that miR-21 and let-7 can serve as ligands of TLRs, activating TLR signaling via the NF-κB pathway.[68–70] Since our study showed that EVs carrying low levels of let-7b and miRNA-21 were less effective in suppressing inflammatory cytokines, it is possible to speculate that the regulatory mechanism of miRNAs in TLR signaling might change depending on the concentration of miRNAs in EVs. Also, we found that manipulation of individual miRNAs in MSCs changed not only the target miRNA but also other key factors. This finding suggests that the decreased regulatory function of the modified EVs lacking let-7b-5p or miR-21-5p could be due to indirect effects mediated by other factors. In this regard, further dose-dependent studies are needed to determine whether miR-21 and let-7b in MSC-EVs directly suppress TCR and TLR signaling by RNA silencing and post-transcriptional regulation of TCR, TLRs, or downstream genes. Nevertheless, our data suggest that the identified key effectors TGFβ1, PTX3, let-7b-5p, or miR-21-5p contribute to the suppressive effect of MSC-EVs and can also serve as signature molecules of functionally effective MSC-EVs.

One of major challenges in developing MSC-based cell therapy is a large variation in therapeutic efficacies of MSCs depending on differences in donors, culture conditions, and tissue sources. Since EVs carry proteins and RNAs of their parent cells, the contents of MSC-EVs would change as do their parent MSCs; therefore, EV-based therapies pose the same challenge of functional variation as MSC therapy. In this regard, our study has important clinical implications in that they provide the following strategies for development of effective and robust MSC-EV therapies. First, early-passage MSCs expanded under a 3D culture system can be used as a cellular source for functionally effective EV production. Our data revealed that EVs from early-passage MSCs exhibited better immunomodulatory potency and they were more effective when produced from 3D culture of the cells than from the conventional 2D culture. From the perspective of clinical translation, our observation of the enhanced regulatory function in 3D MSC-EVs is noteworthy because a 3D culture system also benefits scalable EV production. Although the levels of key effectors PTX3 and miR-21-5p in 2D MSC-EVs were decreased in 3D MSC-EVs in our study, the powerful immunomodulatory cytokine TGF-β1 and TLR4/NF-κB negative regulator let-7b-5p were markedly increased in 3D MSC-EVs. Moreover, 3D MSC-EVs contained a significant amount of the anti-inflammatory protein TSG-6, a key therapeutic factor secreted by activated MSCs.[47,48,71–74] Additionally, our data revealed that many other miRNAs, including miR-125a-5p, a modulator of macrophage polarization,[75] and adhesion molecules (ITGA2 [integrin alpha2], ITGBL1 [integrin subunit beta-like 1), were significantly increased in 3D MSC-EVs. For these reasons, our study suggests that the 3D culture system activates MSCs more efficiently to secrete EVs containing therapeutic factors than does 2D culture. However, further studies are necessary to demonstrate whether these molecules are responsible for the enhanced function of 3D MSC-EVs. Second, the cell density should be considered in the production of functionally effective EVs. We found that the expression levels of the identified key factors in MSC-EVs as well as their regulatory function varied with the cell density of parent cells in culture. Interestingly, there was no change in TGF-β1 mRNA levels in parent cells (data not shown), but TGF-β1 protein levels increased in their EVs when produced from high-density MSCs, indicating that proteins and RNAs can be discriminately transferred into EVs during their biosynthesis. It has been shown that RNAs are packaged into exosomes through a tightly regulated sorting and packaging mechanism.[76,77] However, the mechanisms by which molecules are packaged into exosomes remain unknown, which advocates further research. Third, the identified key effectors TGF-β1, PTX3, let-7b-5p, or miR-21-5p in functionally effective EVs can be used as functional biomarkers for EV production. Since our data clearly showed a strong positive correlation between the levels of TGF-β1, PTX3, let-7b-5p, or miR-21-5p in 2D MSC-EVs and their regulatory potency, we anticipate developing bioassays with these enriched factors to screen a cellular source for EV production and evaluate the regulatory function of MSC-EVs by using simple ELISA or RT-PCR assays. Lastly, the therapeutic potency of MSC-EVs can be enhanced by overexpressing the identified key effectors in MSCs. Our results revealed that the manipulation of TGF-β1, PTX3, let-7b-5p, and miR-21-5p levels in MSCs directly affected the immunomodulatory potency of their EVs. Also, overexpression of TGF-β1 and PTX3 in late-passage MSCs led to production of more effective EVs in suppressing the activation of splenocytes. Therefore, even if late-passage MSCs lose their differentiation potential and show some early signs of genomic instability (Figures S4 and S5), the strategy of overexpressing the key factors in MSCs would help avoid the functional variation of MSC-EVs and potential risks related to clinical use of MSCs extensively expanded *in vitro*. Furthermore, our results showed that simple transfection of cDNA plasmids, siRNA, or miRNA inhibitor into MSCs directly altered the expression level of target protein or miRNA in their EVs. Given that the contents of EVs could be easily manipulated by engineering their parent cells, the platform using MSC-EVs would be applicable for systemic and intracellular delivery of therapeutic proteins.

In summary, we herein provide the pre-clinical data to support the therapeutic applications of MSC-EVs for the treatment of autoimmune disease. Our comparative analysis of molecular profiles of functionally effective MSC-EVs helps understand the molecular mechanisms by which MSC-EVs modulate immune response and presents essential insights into the rational design of EV-based therapies.

MATERIALS AND METHODS

MSC 2D and 3D Cultures

Human MSCs (donors #6015, #7012, and #7075) were obtained from the Center for the Preparation and Distribution of Adult Stem Cells in the Institute for Regenerative Medicine at Texas A&M University, expanded with a low-density seeding method as previously described.[45] The MSCs (donors #6015 and #7012) used in *in vivo* studies were fully characterized in our previous study[45] and Figure S4, respectively. Also, karyotyping of #7012 MSCs was performed in the Molecular Cytogenetics Laboratory of the Department of Veterinary

Integrative Biosciences at Texas A&M University (Figure S5). In order to produce EVs from early- and late-passage MSCs, PD10, PD35, or P40 MSCs were plated at 200 cells/cm^2 in the cell stack with complete culture medium (CCM). After the cells reached about 70% confluency, MSCs were incubated with a medium optimized for Chinese hamster ovary cells (CD-CHO medium, Invitrogen, Carlsbad, CA, USA) for EV production.[78] After 6 h, the medium was discarded and replaced by fresh CD-CHO medium and recovered at 48 h. For 3D culture of MSCs, human MSCs (donor #7012) PD10 (1×10^6 cells) were seeded to 1 g of low-concentration Synthemax II microcarriers (Corning Life Sciences, catalog no. 3781; 360 cm^2, Corning Life Sciences, Corning, NY, USA) with a volume of 15 mL of CCM containing 5% fetal bovine serum (FBS) in a 125-mL spinner flask for the first 24 h. Then CCM was added to cells to a final volume 50 mL for the remaining time according to the manufacturer's protocol. Cultures were incubated at 37°C with agitation at 30 rpm for 5 min every 3 h. Half of the volume medium was replenished every 2 days. On day 7, medium was removed, microcarriers were washed in PBS twice, and 50 mL of CD-CHO medium was added for EV production. After 24 h, the medium was recovered.

Isolation of MSC-EVs and Characterization

For EV isolation, the conditioned medium was filtered to remove cellular debris (0.22 μm), and then EVs were isolated from the supernatant by SEC or ultracentrifugation. In the SEC method, the filtered medium was concentrated by Vivaspin tubes (10 kDa molecular weight cutoff [MWCO], GE Healthcare, Chicago, IL, USA) to 20 mL and applied to a pre-washed column (HansaBioMed, Tallinn, Estonia; catalog ref. maxiPURE-EVs) according to the manufacturer's protocol. A total of 65 fractions of 1.8 mL were collected and the presence of tetraspanin CD63 and protein contents was determined in each fraction by CD63 ELISA (see the ELISA section below) and Bradford assay (Bio-Rad, Hercules, CA, USA), respectively. The fractions containing CD63 (A in Figure 1A) and fractions containing proteins (B in Figure 1A) were combined separately and concentrated with Vivaspin tubes (10 kDa MWCO). In the ultracentrifugation method, the medium was ultracentrifuged at 100,000 × *g* for 16 h at 4°C using a Sorvall WX Floor Ultra Centrifuge with an AH-629 36-mL swinging bucket rotor (Thermo Fisher Scientific, Waltham, MA, USA). EV pellets were resuspended in cold PBS.[3,4] The particle size and number of EVs were analyzed using the NanoSight LM 10 nanoparticle tracking analysis system (Malvern, Malvern, UK) and the Tescan Vega scanning electron microscope (SEM; Tescan, Brno, Czech Republic). The isolated EVs were stored at −80°C until used for molecular profiling, ELISAs, *in vitro* splenocyte assays, and *in vivo* studies.

Protein Profiling

Differential protein profiling was performed in PD15, PD40, and 3D-cultured PD15 MSC-EVs in the Mass Spectrometry Proteomics Core (Baylor College of Medicine, Houston, TX, USA). In brief, proteins were extracted from MSC-EVs and resolved on SDS-PAGE Coomassie blue-stained gels. All bands were identified by mass spectrometry (MS) with the nano-HPLC-ESI-LTQ. Obtained MS/MS spectra were searched against the target-decoy mouse RefSeq database (release 2015_06, containing 58,549 entries) in the Proteome Discoverer 1.4 interface (PD1.4, Thermo Fisher Scientific) with a Mascot algorithm (Mascot 2.4, Matrix Science, London, UK).

Mouse Splenocyte Stimulation

Mouse splenocytes were isolated from BALB/c mice (Jackson Laboratory, Bar Harbor, ME, USA). For T cell activation, the splenocytes (2.5×10^5 cells/well) were incubated in the plate bound with anti-CD3 (Corning Life Sciences) for 24 h or in the plate with anti-CD3/CD28 beads (Thermo Fisher Scientific) for 72 h with or without EVs or commercial recombinant proteins. For LPS stimulation, splenocytes (5×10^5 cells/well) were stimulated with 50 ng/mL LPS (Sigma, St. Louis, MO, USA) for 24 h with or without EVs. One day later, 0.1 mL of cell-free supernatant was harvested to measure cytokine levels by ELISA.

ELISA

For detection of EVs in fractions, CD63 levels in SEC fractions were quantitated in a 96-well plates coated with 5 μg/mL anti-CD63 (clone H5C6, Becton Dickinson, Burlington, NC, USA) utilizing rhCD63 (RayBiotech, Norcross, GA, USA).[78] Mouse IFN-γ, IL-2, IL-6, TNF-α, and Th17A/F in the culture supernatants of splenocytes were measured by commercial ELISA kits (R&D Systems, Minneapolis, MN, USA) according to the manufacturer's protocol. The concentrations of proteins in early-passage, late-passage, and 3D-cultured MSC-EVs (1×10^{10} particles/mL) were measured by commercial ELISA kits (EDIL3, GAL3, LUM, PTX3, TGF-β1, TGF-β2, and TGFβI from R&D Systems, TSG-6 from RayBiotech, and BGN from Invitrogen).

Western Blot Analysis

MSC-EVs (1×10^9 particles/lane) and protein (50 μg/lane) samples were loaded onto a gel. Total protein (50 μg/lane) or nuclear extraction (20 μg/lane) was isolated from anti-CD3/CD28- or LPS-stimulated splenocytes with/without MSC-EVs (3×10^9 particles/mL) for 30 min, 1 h, or 3 h. The following antibodies were used: CD63 (H5C6; Becton Dickinson), CD81 (1.3.3.22; Invitrogen), CD9 (D8O1A), NFAT1, NF-κB p65, p38, phosphorylated (p-)LAT, LAT, TBP (Cell Signaling Technology, Danvers, MA, USA), and β-actin (Invitrogen).

Real-Time PCR Analysis of mRNA and miRNAs and miRNA Profiling

RNA was extracted with an RNeasy mini kit (QIAGEN, Hilden, Germany). The PCR probe and primer sets were purchased from Applied Biosystems (TaqMan gene expression assay; Applied Biosystems, Foster City, CA, USA), and GAPDH was used as the reference RNA. For miRNA sequencing (LC Sciences, Houston, TX, USA), total RNA was isolated from ultracentrifuged EVs (1×10^{11} particles) with the EZNA total RNA kit (Omega Bio-tek, Doraville, CA, USA). For the confirmation of the miRNA sequencing data, miRNA expression levels of let-7b and miR-21-5p were measured by using a TaqMan miRNA reverse transcription kit. The expression of miRNAs in

MSCs was normalized by the expression of U6B, and the expression of miRNAs in EVs was normalized by miR-26b that was consistently expressed in all of the conditions (3D EVs, early-passage EVs, and late-passage EV) in our miRNA sequencing data.

Cell Transfection

When cells reached about 60% confluency, they were transfected with 20 nM siRNA for control, TGF-β1, TGFβI, PTX3, and LUM (Santa Cruz, Dallas, TX, USA) or 30 nM miRNA inhibitors for control, let-7b-5p, and miR-21-5p (Invitrogen), or 0.5 μg/mL DNA plasmids for control, TGF-β1, and PTX3 (OriGene, Rockville, MD, USA) using Lipofectamine (Invitrogen) for 6 h. After transfection, cells were recovered with antibiotic-free CCM overnight. The next day, the cells were treated with CD-CHO medium for collecting EVs.

Mouse Model of Primary Sjögren's Syndrome

Experiments were approved by the Institutional Animal Care and Use Committee at the Seoul National University Hospital. Twelve-week-old NOD.B10.H2^b mice (Jackson Laboratory) were used as a model of ocular Sjögren's syndrome.[41,79] Twelve-week-old C57BL/6 mice (Orient Bio, Seongnam, Korea) were used as controls. For treatment, PBS (20 μL) or MSC-EVs (5×10^8 particles in 20 μL of PBS) were injected into intraorbital lacrimal glands using a 33G syringe (Hamilton, Reno, NV, USA) under an operating microscope (Carl Zeiss, Jena, Germany). The number of EVs (5×10^8 particles per gland) was selected based on our previous study;[44] in this study, we found that intra-lacrimal gland injections of 1×10^3 MSCs and 1×10^5 MSCs were both effective in protecting the ocular surface, with 1×10^5 MSCs being slightly superior to 1×10^3 MSCs. Considering the EV number produced by MSCs (Figure 2C), 5×10^8 EVs were chosen for intra-lacrimal gland injection.

One week later, the corneal epithelial integrity was imaged under a microscope after 3% lissamine green vital staining (Sigma), and the epithelial defects were graded as follows: 0, no punctuate staining; 1, less than one-third of the cornea was stained; 2, two-thirds or less of the cornea was stained; and 3, more than two-thirds of the cornea was stained.[79] Tear production was measured by a phenol red thread test for 60 s (FCI Ophthalmics, Pembroke, MA, USA). The intraorbital lacrimal gland and ocular surface containing the cornea and conjunctiva were extracted and subjected to molecular and histologic assays.

LPS-Stimulated Mouse Model

Experiments were approved by the Institutional Animal Care and Use Committee at Texas A&M University. The 2D- and 3D-cultured MSC-EVs (1×10^{10} particles/mouse) and 30 μg/mouse LPS (Sigma) were injected intravenously into 8-week-old male BALB/c mice (Jackson Laboratory). After 5 h, spleen and blood were collected for assays.

Histology

For PAS staining, the excised tissue was fixed in formalin and sliced through superior and inferior conjunctival fornices. The number of PAS-stained cells (goblet cells) was counted in four different sections of the forniceal conjunctiva from the same animal under a microscope (Leica application suite, version 3.8.0, Leica Microsystems, Heerbrugg, Switzerland), and the average count per section was determined as the goblet cell count. For CD3 immunohistochemical staining, the intraorbital lacrimal gland was stained with a rabbit anti-mouse CD3 (ab5690, Abcam, Cambridge, MA, USA).

Statistical Analysis

All data were analyzed using one-way ANOVA followed by Dunnett's or Tukey's multiple comparison tests. Statistical analysis and graphical generation of data were done with GraphPad Prism software (GraphPad, San Diego, CA, USA).

SUPPLEMENTAL INFORMATION

Supplemental Information can be found online at https://doi.org/10.1016/j.ymthe.2020.04.020.

AUTHOR CONTRIBUTIONS

J.Y.O. and R.H.L. designed research; H.K., M.J.L., J.S.R., E.-H.B., G.K., H.J.K., J.Y.K., H.B., T.S.-K., J.Y.O., and R.H.L. performed experiments; H.K., M.J.L., J.S.R., E.-H.B., S.Y.J., J.M.C., J.Y.O., and R.H.L. analyzed data; J.Y.O. and R.H.L. supervised the project; and H.K., J.Y.O., and R.H.L. wrote the paper.

CONFLICTS OF INTEREST

The authors declare no competing interests.

ACKNOWLEDGMENTS

This work was supported by National Institutes of Health, United States under award numbers R01EY029350 and R21DE027457, and by the National Research Foundation of Korea funded by the Korea government (MSIT) under grant 2018R1A2B2004108.

REFERENCES

1. Reis, M., Mavin, E., Nicholson, L., Green, K., Dickinson, A.M., and Wang, X.N. (2018). Mesenchymal stromal cell-derived extracellular vesicles attenuate dendritic cell maturation and function. Front. Immunol. *9*, 2538.

2. Phinney, D.G., and Pittenger, M.F. (2017). Concise review: MSC-derived exosomes for cell-free therapy. Stem Cells *35*, 851–858.

3. Shigemoto-Kuroda, T., Oh, J.Y., Kim, D.K., Jeong, H.J., Park, S.Y., Lee, H.J., Park, J.W., Kim, T.W., An, S.Y., Prockop, D.J., and Lee, R.H. (2017). MSC-derived extracellular vesicles attenuate immune responses in two autoimmune murine models: type 1 diabetes and uveoretinitis. Stem Cell Reports *8*, 1214–1225.

4. Hai, B., Shigemoto-Kuroda, T., Zhao, Q., Lee, R.H., and Liu, F. (2018). Inhibitory effects of iPSC-MSCs and their extracellular vesicles on the onset of sialadenitis in a mouse model of Sjögren's syndrome. Stem Cells Int. *2018*, 2092315.

5. Kilpinen, L., Impola, U., Sankkila, L., Ritamo, I., Aatonen, M., Kilpinen, S., Tuimala, J., Valmu, L., Levijoki, J., Finckenberg, P., et al. (2013). Extracellular membrane vesicles from umbilical cord blood-derived MSC protect against ischemic acute kidney injury, a feature that is lost after inflammatory conditioning. J. Extracell. Vesicles *2*, https://doi.org/10.3402/jev.v2i0.21927.

6. Ragni, E., Banfi, F., Barilani, M., Cherubini, A., Parazzi, V., Larghi, P., Dolo, V., Bollati, V., and Lazzari, L. (2017). Extracellular vesicle-shuttled mRNA in mesenchymal stem cell communication. Stem Cells *35*, 1093–1105.

7. Zhao, H., Shang, Q., Pan, Z., Bai, Y., Li, Z., Zhang, H., Zhang, Q., Guo, C., Zhang, L., and Wang, Q. (2018). Exosomes from adipose-derived stem cells attenuate adipose inflammation and obesity through polarizing M2 macrophages and beiging in white adipose tissue. Diabetes *67*, 235–247.

8. Blazquez, R., Sanchez-Margallo, F.M., de la Rosa, O., Dalemans, W., Alvarez, V., Tarazona, R., and Casado, J.G. (2014). Immunomodulatory potential of human adipose mesenchymal stem cells derived exosomes on in vitro stimulated T cells. Front. Immunol. *5*, 556.

9. Cho, B.S., Kim, J.O., Ha, D.H., and Yi, Y.W. (2018). Exosomes derived from human adipose tissue-derived mesenchymal stem cells alleviate atopic dermatitis. Stem Cell Res. Ther. *9*, 187.

10. Mokarizadeh, A., Delirezh, N., Morshedi, A., Mosayebi, G., Farshid, A.A., and Mardani, K. (2012). Microvesicles derived from mesenchymal stem cells: potent organelles for induction of tolerogenic signaling. Immunol. Lett. *147*, 47–54.

11. Zhang, B., Yin, Y., Lai, R.C., Tan, S.S., Choo, A.B., and Lim, S.K. (2014). Mesenchymal stem cells secrete immunologically active exosomes. Stem Cells Dev. *23*, 1233–1244.

12. Zhang, B., Yeo, R.W.Y., Lai, R.C., Sim, E.W.K., Chin, K.C., and Lim, S.K. (2018). Mesenchymal stromal cell exosome-enhanced regulatory T-cell production through an antigen-presenting cell-mediated pathway. Cytotherapy *20*, 687–696.

13. Del Fattore, A., Luciano, R., Pascucci, L., Goffredo, B.M., Giorda, E., Scapaticci, M., Fierabracci, A., and Muraca, M. (2015). Immunoregulatory effects of mesenchymal stem cell-derived extracellular vesicles on T lymphocytes. Cell Transplant. *24*, 2615–2627.

14. Chen, W., Huang, Y., Han, J., Yu, L., Li, Y., Lu, Z., Li, H., Liu, Z., Shi, C., Duan, F., and Xiao, Y. (2016). Immunomodulatory effects of mesenchymal stromal cells-derived exosome. Immunol. Res. *64*, 831–840.

15. Hyvärinen, K., Holopainen, M., Skirdenko, V., Ruhanen, H., Lehenkari, P., Korhonen, M., Käkelä, R., Laitinen, S., and Kerkelä, E. (2018). Mesenchymal stromal cells and their extracellular vesicles enhance the anti-inflammatory phenotype of regulatory macrophages by downregulating the production of interleukin (IL)-23 and IL-22. Front. Immunol. *9*, 771.

16. Morrison, T.J., Jackson, M.V., Cunningham, E.K., Kissenpfennig, A., McAuley, D.F., O'Kane, C.M., and Krasnodembskaya, A.D. (2017). Mesenchymal stromal cells modulate macrophages in clinically relevant lung injury models by extracellular vesicle mitochondrial transfer. Am. J. Respir. Crit. Care Med. *196*, 1275–1286.

17. Lo Sicco, C., Reverberi, D., Balbi, C., Ulivi, V., Principi, E., Pascucci, L., Becherini, P., Bosco, M.C., Varesio, L., Franzin, C., et al. (2017). Mesenchymal stem cell-derived extracellular vesicles as mediators of anti-inflammatory effects: endorsement of macrophage polarization. Stem Cells Transl. Med. *6*, 1018–1028.

18. Chamberlain, C.S., Clements, A.E.B., Kink, J.A., Choi, U., Baer, G.S., Halanski, M.A., Hematti, P., and Vanderby, R. (2019). Extracellular vesicle-educated macrophages promote early achilles tendon healing. Stem Cells *37*, 652–662.

19. Chen, T.S., Lai, R.C., Lee, M.M., Choo, A.B., Lee, C.N., and Lim, S.K. (2010). Mesenchymal stem cell secretes microparticles enriched in pre-microRNAs. Nucleic Acids Res. *38*, 215–224.

20. Vallabhaneni, K.C., Penfornis, P., Dhule, S., Guillonneau, F., Adams, K.V., Mo, Y.Y., Xu, R., Liu, Y., Watabe, K., Vemuri, M.C., and Pochampally, R. (2015). Extracellular vesicles from bone marrow mesenchymal stem/stromal cells transport tumor regulatory microRNA, proteins, and metabolites. Oncotarget *6*, 4953–4967.

21. Eirin, A., Riester, S.M., Zhu, X.Y., Tang, H., Evans, J.M., O'Brien, D., van Wijnen, A.J., and Lerman, L.O. (2014). MicroRNA and mRNA cargo of extracellular vesicles from porcine adipose tissue-derived mesenchymal stem cells. Gene *551*, 55–64.

22. Eirin, A., Zhu, X.Y., Puranik, A.S., Woollard, J.R., Tang, H., Dasari, S., Lerman, A., van Wijnen, A.J., and Lerman, L.O. (2016). Comparative proteomic analysis of extracellular vesicles isolated from porcine adipose tissue-derived mesenchymal stem/stromal cells. Sci. Rep. *6*, 36120.

23. Anderson, J.D., Johansson, H.J., Graham, C.S., Vesterlund, M., Pham, M.T., Bramlett, C.S., Montgomery, E.N., Mellema, M.S., Bardini, R.L., Contreras, Z., et al. (2016). Comprehensive proteomic analysis of mesenchymal stem cell exosomes reveals modulation of angiogenesis via nuclear factor-kappaB signaling. Stem Cells *34*, 601–613.

24. Kim, H.S., Choi, D.Y., Yun, S.J., Choi, S.M., Kang, J.W., Jung, J.W., Hwang, D., Kim, K.P., and Kim, D.W. (2012). Proteomic analysis of microvesicles derived from human mesenchymal stem cells. J. Proteome Res. *11*, 839–849.

25. Lai, R.C., Tan, S.S., Teh, B.J., Sze, S.K., Arslan, F., de Kleijn, D.P., Choo, A., and Lim, S.K. (2012). Proteolytic potential of the MSC exosome proteome: implications for an exosome-mediated delivery of therapeutic proteasome. Int. J. Proteomics *2012*, 971907.

26. Ferguson, S.W., Wang, J., Lee, C.J., Liu, M., Neelamegham, S., Canty, J.M., and Nguyen, J. (2018). The microRNA regulatory landscape of MSC-derived exosomes: a systems view. Sci. Rep. *8*, 1419.

27. Toh, W.S., Lai, R.C., Zhang, B., and Lim, S.K. (2018). MSC exosome works through a protein-based mechanism of action. Biochem. Soc. Trans. *46*, 843–853.

28. Bruno, S., Grange, C., Deregibus, M.C., Calogero, R.A., Saviozzi, S., Collino, F., Morando, L., Busca, A., Falda, M., Bussolati, B., et al. (2009). Mesenchymal stem cell-derived microvesicles protect against acute tubular injury. J. Am. Soc. Nephrol. *20*, 1053–1067.

29. Xin, H., Li, Y., Liu, Z., Wang, X., Shang, X., Cui, Y., Zhang, Z.G., and Chopp, M. (2013). miR-133b promotes neural plasticity and functional recovery after treatment of stroke with multipotent mesenchymal stromal cells in rats via transfer of exosome-enriched extracellular particles. Stem Cells *31*, 2737–2746.

30. Xin, H., Li, Y., Buller, B., Katakowski, M., Zhang, Y., Wang, X., Shang, X., Zhang, Z.G., and Chopp, M. (2012). Exosome-mediated transfer of miR-133b from multipotent mesenchymal stromal cells to neural cells contributes to neurite outgrowth. Stem Cells *30*, 1556–1564.

31. Zhu, Y.G., Feng, X.M., Abbott, J., Fang, X.H., Hao, Q., Monsel, A., Qu, J.M., Matthay, M.A., and Lee, J.W. (2014). Human mesenchymal stem cell microvesicles for treatment of *Escherichia coli* endotoxin-induced acute lung injury in mice. Stem Cells *32*, 116–125.

32. Reza-Zaldivar, E.E., Hernández-Sapiéns, M.A., Minjarez, B., Gutiérrez-Mercado, Y.K., Márquez-Aguirre, A.L., and Canales-Aguirre, A.A. (2018). Potential effects of MSC-derived exosomes in neuroplasticity in Alzheimer's disease. Front. Cell. Neurosci. *12*, 317.

33. Qiu, G., Zheng, G., Ge, M., Wang, J., Huang, R., Shu, Q., and Xu, J. (2018). Mesenchymal stem cell-derived extracellular vesicles affect disease outcomes via transfer of microRNAs. Stem Cell Res. Ther. *9*, 320.

34. Perets, N., Hertz, S., London, M., and Offen, D. (2018). Intranasal administration of exosomes derived from mesenchymal stem cells ameliorates autistic-like behaviors of BTBR mice. Mol. Autism *9*, 57.

35. Digirolamo, C.M., Stokes, D., Colter, D., Phinney, D.G., Class, R., and Prockop, D.J. (1999). Propagation and senescence of human marrow stromal cells in culture: a simple colony-forming assay identifies samples with the greatest potential to propagate and differentiate. Br. J. Haematol. *107*, 275–281.

36. Despars, G., Carbonneau, C.L., Bardeau, P., Coutu, D.L., and Beauséjour, C.M. (2013). Loss of the osteogenic differentiation potential during senescence is limited to bone progenitor cells and is dependent on p53. PLoS ONE *8*, e73206.

37. Zhou, Y., Chen, H., Li, H., and Wu, Y. (2017). 3D culture increases pluripotent gene expression in mesenchymal stem cells through relaxation of cytoskeleton tension. J. Cell. Mol. Med. *21*, 1073–1084.

38. Yokosuka, T., Takamatsu, M., Kobayashi-Imanishi, W., Hashimoto-Tane, A., Azuma, M., and Saito, T. (2012). Programmed cell death 1 forms negative costimulatory microclusters that directly inhibit T cell receptor signaling by recruiting phosphatase SHP2. J. Exp. Med. *209*, 1201–1217.

39. Berger, C., Blau, C.A., Clackson, T., Riddell, S.R., and Heimfeld, S. (2003). CD28 costimulation and immunoaffinity-based selection efficiently generate primary gene-modified T cells for adoptive immunotherapy. Blood *101*, 476–484.

40. Reynolds, J.M., Martinez, G.J., Chung, Y., and Dong, C. (2012). Toll-like receptor 4 signaling in T cells promotes autoimmune inflammation. Proc. Natl. Acad. Sci. USA *109*, 13064–13069.

41. Doyle, M.E., Boggs, L., Attia, R., Cooper, L.R., Saban, D.R., Nguyen, C.Q., and Peck, A.B. (2007). Autoimmune dacryoadenitis of NOD/LtJ mice and its subsequent effects on tear protein composition. Am. J. Pathol. *171*, 1224–1236.

42. Nocturne, G., and Mariette, X. (2013). Advances in understanding the pathogenesis of primary Sjögren's syndrome. Nat. Rev. Rheumatol. *9*, 544–556.

43. Kiripolsky, J., Romano, R.A., Kasperek, E.M., Yu, G., and Kramer, J.M. (2020). Activation of Myd88-dependent TLRs mediates local and systemic inflammation in a mouse model of primary Sjögren's syndrome. Front. Immunol. *10*, 2963.

44. Lee, M.J., Ko, A.Y., Ko, J.H., Lee, H.J., Kim, M.K., Wee, W.R., Khwarg, S.I., and Oh, J.Y. (2015). Mesenchymal stem/stromal cells protect the ocular surface by suppressing inflammation in an experimental dry eye. Mol. Ther. *23*, 139–146.

45. Lee, R.H., Yu, J.M., Foskett, A.M., Peltier, G., Reneau, J.C., Bazhanov, N., Oh, J.Y., and Prockop, D.J. (2014). TSG-6 as a biomarker to predict efficacy of human mesenchymal stem/progenitor cells (hMSCs) in modulating sterile inflammation in vivo. Proc. Natl. Acad. Sci. USA *111*, 16766–16771.

46. Mi, H., Muruganujan, A., Casagrande, J.T., and Thomas, P.D. (2013). Large-scale gene function analysis with the PANTHER classification system. Nat. Protoc. *8*, 1551–1566.

47. Bartosh, T.J., Ylöstalo, J.H., Mohammadipoor, A., Bazhanov, N., Coble, K., Claypool, K., Lee, R.H., Choi, H., and Prockop, D.J. (2010). Aggregation of human mesenchymal stromal cells (MSCs) into 3D spheroids enhances their antiinflammatory properties. Proc. Natl. Acad. Sci. USA *107*, 13724–13729.

48. Lee, R.H., Pulin, A.A., Seo, M.J., Kota, D.J., Ylostalo, J., Larson, B.L., Semprun-Prieto, L., Delafontaine, P., and Prockop, D.J. (2009). Intravenous hMSCs improve myocardial infarction in mice because cells embolized in lung are activated to secrete the anti-inflammatory protein TSG-6. Cell Stem Cell *5*, 54–63.

49. Crabtree, G.R., and Clipstone, N.A. (1994). Signal transmission between the plasma membrane and nucleus of T lymphocytes. Annu. Rev. Biochem. *63*, 1045–1083.

50. Schindler, C., and Darnell, J.E., Jr. (1995). Transcriptional responses to polypeptide ligands: the JAK-STAT pathway. Annu. Rev. Biochem. *64*, 621–651.

51. Balagopalan, L., Kortum, R.L., Coussens, N.P., Barr, V.A., and Samelson, L.E. (2015). The linker for activation of T cells (LAT) signaling hub: from signaling complexes to microclusters. J. Biol. Chem. *290*, 26422–26429.

52. An, H., Yu, Y., Zhang, M., Xu, H., Qi, R., Yan, X., Liu, S., Wang, W., Guo, Z., Guo, J., et al. (2002). Involvement of ERK, p38 and NF-κB signal transduction in regulation of TLR2, TLR4 and TLR9 gene expression induced by lipopolysaccharide in mouse dendritic cells. Immunology *106*, 38–45.

53. Kawai, T., and Akira, S. (2007). Signaling to NF-κB by Toll-like receptors. Trends Mol. Med. *13*, 460–469.

54. Bommireddy, R., and Doetschman, T. (2007). TGFβ1 and Treg cells: alliance for tolerance. Trends Mol. Med. *13*, 492–501.

55. Das, L., and Levine, A.D. (2008). TGF-β inhibits IL-2 production and promotes cell cycle arrest in TCR-activated effector/memory T cells in the presence of sustained TCR signal transduction. J. Immunol. *180*, 1490–1498.

56. Huang, X.L., Zhang, L., Duan, Y., Wang, Y.J., and Wang, J. (2016). Association of pentraxin 3 with autoimmune diseases: a systematic review and meta-analysis. Arch. Med. Res. *47*, 223–231.

57. Balhara, J., Shan, L., Zhang, J., Muhuri, A., Halayko, A.J., Almiski, M.S., Doeing, D., McConville, J., Matzuk, M.M., and Gounni, A.S. (2017). Pentraxin 3 deletion aggravates allergic inflammation through a T_H17-dominant phenotype and enhanced CD4 T-cell survival. J. Allergy Clin. Immunol. *139*, 950–963.e9.

58. Okoye, I.S., Coomes, S.M., Pelly, V.S., Czieso, S., Papayannopoulos, V., Tolmachova, T., Seabra, M.C., and Wilson, M.S. (2014). MicroRNA-containing T-regulatory-cell-derived exosomes suppress pathogenic T helper 1 cells. Immunity *41*, 89–103.

59. Swaminathan, S., Suzuki, K., Seddiki, N., Kaplan, W., Cowley, M.J., Hood, C.L., Clancy, J.L., Murray, D.D., Méndez, C., Gelgor, L., et al. (2012). Differential regulation of the Let-7 family of microRNAs in $CD4^+$ T cells alters IL-10 expression. J. Immunol. *188*, 6238–6246.

60. Hsieh, C.H., Tai, S.K., and Yang, M.H. (2018). Snail-overexpressing cancer cells promote M2-like polarization of tumor-associated macrophages by delivering miR-21-abundant exosomes. Neoplasia *20*, 775–788.

61. Ti, D., Hao, H., Tong, C., Liu, J., Dong, L., Zheng, J., Zhao, Y., Liu, H., Fu, X., and Han, W. (2015). LPS-preconditioned mesenchymal stromal cells modify macrophage polarization for resolution of chronic inflammation via exosome-shuttled let-7b. J. Transl. Med. *13*, 308.

62. Wang, Z., Xu, L., Hu, Y., Huang, Y., Zhang, Y., Zheng, X., Wang, S., Wang, Y., Yu, Y., Zhang, M., et al. (2016). miRNA let-7b modulates macrophage polarization and enhances tumor-associated macrophages to promote angiogenesis and mobility in prostate cancer. Sci. Rep. *6*, 25602.

63. Zhu, W.D., Xu, J., Zhang, M., Zhu, T.M., Zhang, Y.H., and Sun, K. (2018). MicroRNA-21 inhibits lipopolysaccharide-induced acute lung injury by targeting nuclear factor-κB. Exp. Ther. Med. *16*, 4616–4622.

64. Zhao, Z., Hao, J., Li, X., Chen, Y., and Qi, X. (2019). miR-21-5p regulates mycobacterial survival and inflammatory responses by targeting Bcl-2 and TLR4 in *Mycobacterium tuberculosis*-infected macrophages. FEBS Lett. *593*, 1326–1335.

65. Yu, H.R., Hsu, T.Y., Huang, H.C., Kuo, H.C., Li, S.C., Yang, K.D., and Hsieh, K.S. (2016). Comparison of the functional microRNA expression in immune cell subsets of neonates and adults. Front. Immunol. *7*, 615.

66. Nematian, S.E., Mamillapalli, R., Kadakia, T.S., Majidi Zolbin, M., Moustafa, S., and Taylor, H.S. (2018). Systemic inflammation induced by microRNAs: endometriosis-derived alterations in circulating microRNA 125b-5p and Let-7b-5p regulate macrophage cytokine production. J. Clin. Endocrinol. Metab. *103*, 64–74.

67. Teng, G.G., Wang, W.H., Dai, Y., Wang, S.J., Chu, Y.X., and Li, J. (2013). Let-7b is involved in the inflammation and immune responses associated with Helicobacter pylori infection by targeting Toll-like receptor 4. PLoS ONE *8*, e56709.

68. He, X., Jing, Z., and Cheng, G. (2014). MicroRNAs: new regulators of Toll-like receptor signalling pathways. BioMed Res. Int. *2014*, 945169.

69. Fabbri, M., Paone, A., Calore, F., Galli, R., Gaudio, E., Santhanam, R., Lovat, F., Fadda, P., Mao, C., Nuovo, G.J., et al. (2012). MicroRNAs bind to Toll-like receptors to induce prometastatic inflammatory response. Proc. Natl. Acad. Sci. USA *109*, E2110–E2116.

70. Lehmann, S.M., Krüger, C., Park, B., Derkow, K., Rosenberger, K., Baumgart, J., Trimbuch, T., Eom, G., Hinz, M., Kaul, D., et al. (2012). An unconventional role for miRNA: let-7 activates Toll-like receptor 7 and causes neurodegeneration. Nat. Neurosci. *15*, 827–835.

71. Ko, J.H., Lee, H.J., Jeong, H.J., Kim, M.K., Wee, W.R., Yoon, S.O., Choi, H., Prockop, D.J., and Oh, J.Y. (2016). Mesenchymal stem/stromal cells precondition lung monocytes/macrophages to produce tolerance against allo- and autoimmunity in the eye. Proc. Natl. Acad. Sci. USA *113*, 158–163.

72. Kota, D.J., Wiggins, L.L., Yoon, N., and Lee, R.H. (2013). TSG-6 produced by hMSCs delays the onset of autoimmune diabetes by suppressing Th1 development and enhancing tolerogenicity. Diabetes *62*, 2048–2058.

73. Roddy, G.W., Oh, J.Y., Lee, R.H., Bartosh, T.J., Ylostalo, J., Coble, K., Rosa, R.H., Jr., and Prockop, D.J. (2011). Action at a distance: systemically administered adult stem/progenitor cells (MSCs) reduce inflammatory damage to the cornea without engraftment and primarily by secretion of TNF-α stimulated gene/protein 6. Stem Cells *29*, 1572–1579.

74. Choi, H., Lee, R.H., Bazhanov, N., Oh, J.Y., and Prockop, D.J. (2011). Anti-inflammatory protein TSG-6 secreted by activated MSCs attenuates zymosan-induced mouse peritonitis by decreasing TLR2/NF-κB signaling in resident macrophages. Blood *118*, 330–338.

75. Banerjee, S., Cui, H., Xie, N., Tan, Z., Yang, S., Icyuz, M., Thannickal, V.J., Abraham, E., and Liu, G. (2013). miR-125a-5p regulates differential activation of macrophages and inflammation. J. Biol. Chem. *288*, 35428–35436.

76. Mateescu, B., Kowal, E.J., van Balkom, B.W., Bartel, S., Bhattacharyya, S.N., Buzás, E.I., Buck, A.H., de Candia, P., Chow, F.W., Das, S., et al. (2017). Obstacles and opportunities in the functional analysis of extracellular vesicle RNA—an ISEV position paper. J. Extracell. Vesicles *6*, 1286095.

77. Ragusa, M., Statello, L., Maugeri, M., Barbagallo, C., Passanisi, R., Alhamdani, M.S., Li Destri, G., Cappellani, A., Barbagallo, D., Scalia, M., et al. (2014). Highly skewed distribution of miRNAs and proteins between colorectal cancer cells and their exosomes following cetuximab treatment: biomolecular, genetic and translational implications. Oncoscience *1*, 132–157.

78. Kim, D.K., Nishida, H., An, S.Y., Shetty, A.K., Bartosh, T.J., and Prockop, D.J. (2016). Chromatographically isolated CD63+CD81+ extracellular vesicles from mesenchymal stromal cells rescue cognitive impairments after TBI. Proc. Natl. Acad. Sci. USA *113*, 170–175.

79. Lee, M.J., Kim, D.H., Ryu, J.S., Ko, A.Y., Ko, J.H., Kim, M.K., Wee, W.R., Khwarg, S.I., and Oh, J.Y. (2015). Topical TSG-6 administration protects the ocular surface in two mouse models of inflammation-related dry eye. Invest. Ophthalmol. Vis. Sci. *56*, 5175–5181.

YMTHE, Volume *28*

Supplemental Information

Comprehensive Molecular Profiles of Functionally Effective MSC-Derived Extracellular Vesicles in Immunomodulation

Hyemee Kim, Min Joung Lee, Eun-Hye Bae, Jin Suk Ryu, Gagandeep Kaur, Hyeon Ji Kim, Jun Yeob Kim, Heather Barreda, Sung Youn Jung, Jong Min Choi, Taeko Shigemoto-Kuroda, Joo Youn Oh, and Ryang Hwa Lee

Supplemental Table 1. KEGG pathway ranking summary of predicted targets of let-7b-5p and miR-21a-5p.

TERM	TERM_ID	TOTAL_GENES_OF_THE_TERM	UNION_TARGETS_IN_THE_TERM	MIRS_IN_THE_TERM	SCORE
MAPK_SIGNALING_PATHWAY	4010	271	39	2	6.802
PATHWAYS_IN_CANCER	5200	323	35	2	3.962
NEUROTROPHIN_SIGNALING_PATHWAY	4722	131	17	2	3.229
AXON_GUIDANCE	4360	131	18	2	3.137
JAK-STAT_SIGNALING_PATHWAY	4630	153	18	2	2.698
TGF-BETA_SIGNALING_PATHWAY	4350	85	11	2	2.533
FOCAL_ADHESION	4510	197	21	2	2.424
CYTOKINE-CYTOKINE_RECEPTOR_INTERACTION	4060	262	20	2	2.195
MELANOMA	5218	71	11	2	2.173
ENDOCYTOSIS	4144	219	19	2	2.113
COLORECTAL_CANCER	5210	65	9	2	2.07
WNT_SIGNALING_PATHWAY	4310	153	16	2	2.048
INSULIN_SIGNALING_PATHWAY	4910	137	15	2	1.996
REGULATION_OF_ACTIN_CYTOSKELETON	4810	215	17	2	1.906
NOTCH_SIGNALING_PATHWAY	4330	49	7	2	1.835
PROSTATE_CANCER	5215	89	11	2	1.835
CHEMOKINE_SIGNALING_PATHWAY	4062	187	15	2	1.785
ENDOMETRIAL_CANCER	5213	52	8	2	1.756
MTOR_SIGNALING_PATHWAY	4150	53	8	2	1.756
PANCREATIC_CANCER	5212	70	9	2	1.748
GLIOMA	5214	65	9	2	1.71
BASAL_CELL_CARCINOMA	5217	55	8	2	1.683
T_CELL_RECEPTOR_SIGNALING_PATHWAY	4660	109	10	2	1.663
UBIQUITIN_MEDIATED_PROTEOLYSIS	4120	138	11	2	1.653
CHAGAS_DISEASE	5142	102	9	2	1.615
PROTEIN_PROCESSING_IN_ENDOPLASMIC_RETICULUM	4141	167	12	2	1.585
TOXOPLASMOSIS	5145	128	12	2	1.577
CHRONIC_MYELOID_LEUKEMIA	5220	73	9	2	1.548
BLADDER_CANCER	5219	42	6	1	1.427
ADIPOCYTOKINE_SIGNALING_PATHWAY	4920	68	7	2	1.424
GNRH_SIGNALING_PATHWAY	4912	99	9	2	1.395

AMOEBIASIS	5146	115	11	2	1.387
MELANOGENESIS	4916	100	10	2	1.382
SPLICEOSOME	3040	126	7	2	1.365
B_CELL_RECEPTOR_SIGNALING_PATHWAY	4662	76	7	2	1.348
ERBB_SIGNALING_PATHWAY	4012	87	9	2	1.345
BACTERIAL_INVASION_OF_EPITHELIAL_CELLS	5100	71	6	2	1.338
PROTEIN_DIGESTION_AND_ABSORPTION	4974	75	8	2	1.328
HEPATITIS_C	5160	137	8	2	1.248
BASAL_TRANSCRIPTION_FACTORS	3022	36	4	2	1.192
TYPE_II_DIABETES_MELLITUS	4930	49	6	2	1.191
SMALL_CELL_LUNG_CANCER	5222	85	8	2	1.185
APOPTOSIS	4210	86	7	2	1.173
PROGESTERONE-MEDIATED_OOCYTE_MATURATION	4914	87	7	2	1.162
P53_SIGNALING_PATHWAY	4115	69	7	2	1.149
VEGF_SIGNALING_PATHWAY	4370	76	7	2	1.129
NATURAL_KILLER_CELL_MEDIATED_CYTOTOXICITY	4650	150	10	2	1.122
NON-SMALL_CELL_LUNG_CANCER	5223	54	6	2	1.102
RENAL_CELL_CARCINOMA	5211	71	7	2	1.088
TYPE_I_DIABETES_MELLITUS	4940	59	4	2	1.076
RIG-I-LIKE_RECEPTOR_SIGNALING_PATHWAY	4622	69	5	2	1.072
FC_GAMMA_R-MEDIATED_PHAGOCYTOSIS	4666	90	8	2	1.071
ACUTE_MYELOID_LEUKEMIA	5221	57	6	2	1.063
ADHERENS_JUNCTION	4520	74	7	2	1.051
GLYCOSPHINGOLIPID_BIOSYNTHESIS_LACTO_AND_NEOLACTO_SERIES	601	26	4	2	1.043
GLYCEROPHOSPHOLIPID_METABOLISM	564	79	7	2	1.03
PPAR_SIGNALING_PATHWAY	3320	80	6	2	1.019
FC_EPSILON_RI_SIGNALING_PATHWAY	4664	80	7	2	0.986
ALLOGRAFT_REJECTION	5330	52	4	2	0.933
CELL_ADHESION_MOLECULES_(CAMS)	4514	149	2	2	0.927
TOLL-LIKE_RECEPTOR_SIGNALING_PATHWAY	4620	101	7	2	0.921
HEDGEHOG_SIGNALING_PATHWAY	4340	54	5	2	0.91

LONG-TERM_DEPRESSION	4730	72	6	1	0.891
CELL_CYCLE	4110	125	7	2	0.873
LYSOSOME	4142	121	8	1	0.843
LEUKOCYTE_TRANSENDOTHELIAL_MIGRATION	4670	120	3	2	0.831
NOD-LIKE_RECEPTOR_SIGNALING_PATHWAY	4621	62	5	2	0.831
AMYOTROPHIC_LATERAL_SCLEROSIS_(ALS)	5014	56	5	2	0.83
ECM-RECEPTOR_INTERACTION	4512	83	6	2	0.796
CALCIUM_SIGNALING_PATHWAY	4020	178	10	1	0.789
NEUROACTIVE_LIGAND-RECEPTOR_INTERACTION	4080	320	12	2	0.781
LYSINE_DEGRADATION	310	43	4	2	0.753
SYSTEMIC_LUPUS_ERYTHEMATOSUS	5322	150	3	2	0.746
ALDOSTERONE-REGULATED_SODIUM_REABSORPTION	4960	44	4	2	0.742
PHAGOSOME	4145	174	4	2	0.74
HYPERTROPHIC_CARDIOMYOPATHY_(HCM)	5410	87	6	1	0.738
ABC_TRANSPORTERS	2010	45	4	2	0.731
GALACTOSE_METABOLISM	52	27	3	2	0.729
PHOSPHATIDYLINOSITOL_SIGNALING_SYSTEM	4070	78	5	2	0.727
VASCULAR_SMOOTH_MUSCLE_CONTRACTION	4270	133	7	2	0.72
VIRAL_MYOCARDITIS	5416	89	6	1	0.72
GLYCOSAMINOGLYCAN_BIOSYNTHESIS_HEPARAN_SULFATE	534	26	3	1	0.719
ALZHEIMER'S_DISEASE	5010	179	5	2	0.692
LONG-TERM_POTENTIATION	4720	69	5	1	0.692
O-GLYCAN_BIOSYNTHESIS	512	28	3	1	0.682
HUNTINGTON'S_DISEASE	5016	189	2	1	0.655
GRAFT-VERSUS-HOST_DISEASE	5332	54	3	2	0.654
MALARIA	5144	54	4	2	0.654
THYROID_CANCER	5216	30	3	1	0.649
PARKINSON'S_DISEASE	5012	141	1	1	0.63
RNA_TRANSPORT	3013	150	5	2	0.616
LEISHMANIASIS	5140	65	4	2	0.592
TIGHT_JUNCTION	4530	135	5	2	0.592
AUTOIMMUNE_THYROID_DISEASE	5320	67	3	2	0.584
HEMATOPOIETIC_CELL_LINEAGE	4640	83	2	2	0.567

PANCREATIC_SECRETION	4972	105	4	2	0.543
COMPLEMENT_AND_COAGULATION_CASCADES	4610	76	2	2	0.541
INOSITOL_PHOSPHATE_METABOLISM	562	57	3	2	0.515
PEROXISOME	4146	80	3	2	0.507
RNA_DEGRADATION	3018	58	2	2	0.491
CARBOHYDRATE_DIGESTION_AND_ABSORPTION	4973	39	2	2	0.487
INTESTINAL_IMMUNE_NETWORK_FOR_IGA_PRODUCTION	4672	44	3	1	0.486
VASOPRESSIN-REGULATED_WATER_REABSORPTION	4962	43	2	2	0.482
AMINO_SUGAR_AND_NUCLEOTIDE_SUGAR_METABOLISM	520	47	2	2	0.48
OOCYTE_MEIOSIS	4114	112	5	1	0.443
N-GLYCAN_BIOSYNTHESIS	510	50	3	1	0.442
PURINE_METABOLISM	230	165	3	1	0.432
BIOSYNTHESIS_OF_UNSATURATED_FATTY_ACIDS	1040	25	2	1	0.43
CYTOSOLIC_DNA-SENSING_PATHWAY	4623	55	3	1	0.412
DILATED_CARDIOMYOPATHY	5414	89	4	1	0.408
GAP_JUNCTION	4540	88	1	1	0.373
ETHER_LIPID_METABOLISM	565	35	2	1	0.349
PRION_DISEASES	5020	35	2	1	0.349
SNARE_INTERACTIONS_IN_VESICULAR_TRANSPORT	4130	35	2	1	0.349
ARRHYTHMOGENIC_RIGHT_VENTRICULAR_CARDIOMYOPATHY_(ARVC)	5412	74	3	1	0.344
SALIVARY_SECRETION	4970	77	3	1	0.338
PYRIMIDINE_METABOLISM	240	98	3	1	0.321
SPHINGOLIPID_METABOLISM	600	41	2	1	0.32
PENTOSE_PHOSPHATE_PATHWAY	30	28	1	1	0.314
GASTRIC_ACID_SECRETION	4971	73	1	1	0.312
LINOLEIC_ACID_METABOLISM	591	45	2	1	0.306
BUTANOATE_METABOLISM	650	30	1	1	0.304
ARACHIDONIC_ACID_METABOLISM	590	86	2	1	0.3
ALANINE_ASPARTATE_AND_GLUTAMATE_METABOLISM	250	32	1	1	0.295
STAPHYLOCOCCUS_AUREUS_INFECTION	5150	51	2	1	0.292
CARDIAC_MUSCLE_CONTRACTION	4260	79	2	1	0.289

ARGININE_AND_PROLINE_METABOLISM	330	53	2	1	0.288
RETINOL_METABOLISM	830	77	2	1	0.287
AMINOACYL-TRNA_BIOSYNTHESIS	970	64	1	1	0.28
FRUCTOSE_AND_MANNOSE_METABOLISM	51	36	1	1	0.279
CYSTEINE_AND_METHIONINE_METABOLISM	270	38	1	1	0.272
GLUTATHIONE_METABOLISM	480	54	1	1	0.249
GLYCEROLIPID_METABOLISM	561	50	1	1	0.238
FATTY_ACID_METABOLISM	71	47	1	1	0.232
GLYCOLYSIS_GLUCONEOGENESIS	10	60	1	1	0.228
STARCH_AND_SUCROSE_METABOLISM	500	44	1	1	0.226
NUCLEOTIDE_EXCISION_REPAIR	3420	43	1	1	0.224
GLYCOSYLPHOSPHATIDYLINOSITOL(GPI)-ANCHOR_BIOSYNTHESIS	563	25	1	1	0.22
ANTIGEN_PROCESSING_AND_PRESENTATION	4612	78	1	1	0.217
BASE_EXCISION_REPAIR	3410	38	1	1	0.217
RNA_POLYMERASE	3020	28	1	1	0.216
PHOTOTRANSDUCTION	4744	29	1	1	0.215
CITRATE_CYCLE_(TCA_CYCLE)	20	32	1	1	0.214
GLYCINE_SERINE_AND_THREONINE_METABOLISM	260	34	1	1	0.214
REGULATION_OF_AUTOPHAGY	4140	35	1	1	0.214

Supplemental Figure 1. Characterization of MSC-EVs isolated by a size exclusion chromatography method. a Particle sizes of MSC conditioned medium and purified MSC-EVs were analyzed by nanoparticle tracking system. **b** Western blot assays with EVs and protein fractions using CD63, CD81, and CD9 antibodies. **c-d** Particle sizes and electron microscopy images of MSC-EVs before and after storage at -80°C.

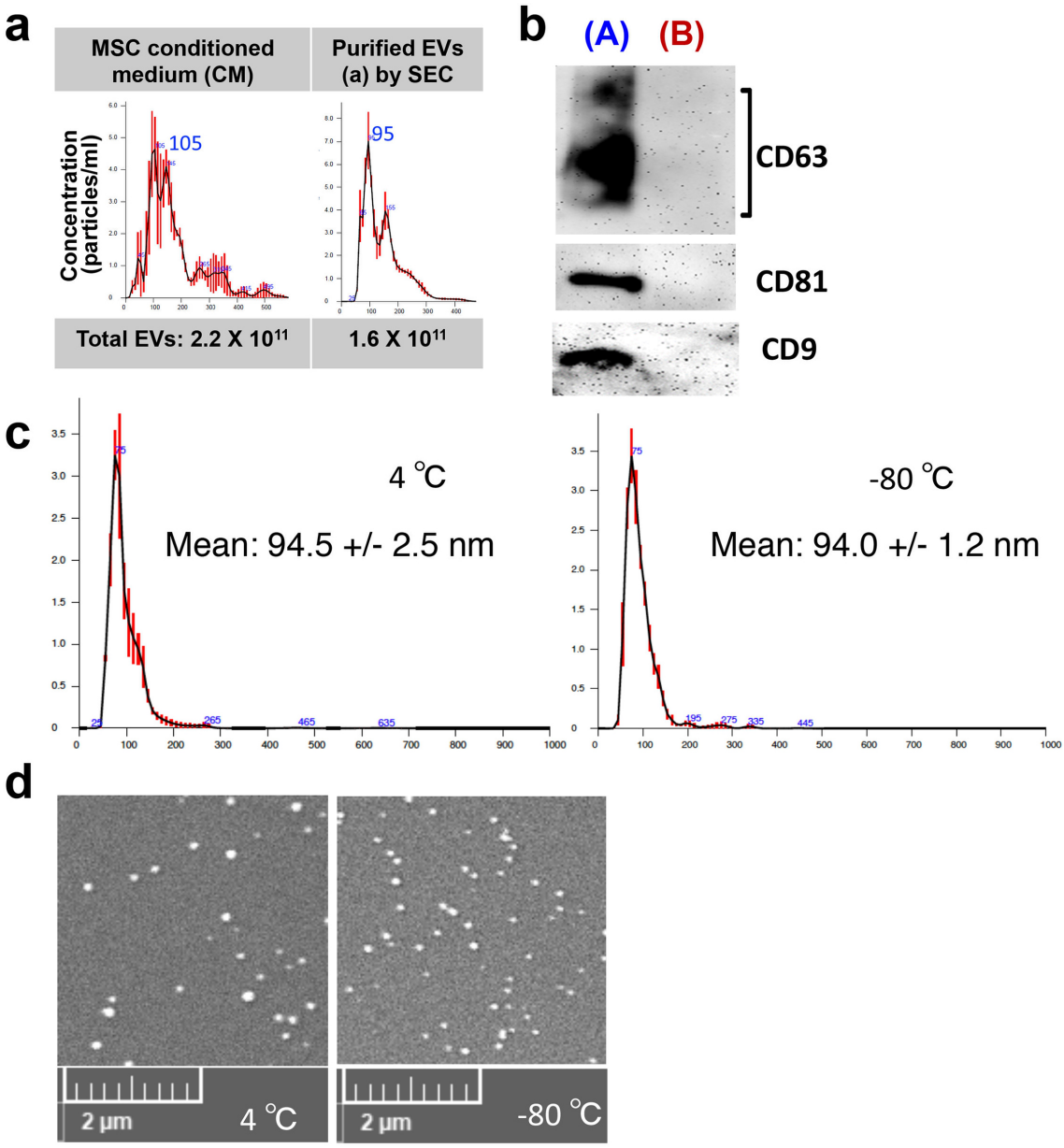

Supplemental Figure 2. Supporting data for the results in Figure 6. a Relative quantification (RQ) of TGFβ1, TGFβI, PTX3 and LUM mRNAs in PD15 MSCs after target siRNAs transfection by RT-PCR assays. **b** RQ of TGFβ1 and PTX3 mRNAs in PD15 MSCs after target DNA plasmid transfection by RT-PCR assays. **c** RQ of TGFβ1 and PTX3 protein levels in EVs by ELISAs. EVs were isolated from PD15 MSCs after target DNA plasmid transfection. **d** IL-2 ELISA with conditioned medium of splenocytes activated by plate-bound anti-CD3 and **e** IL-17 ELISA with conditioned medium of LPS stimulated splenocytes for 24 h with EVs derived from PD15 MSCs transfected with target DNA plasmids (n=4). All data are presented as means ± SD.; *p < 0.05, **p < 0.01, ***p < 0.001, ****p < 0.0001 by one-way ANOVA with Tukey's test. **f** TGFβ1 and PTX3 ELISAs in conditioned medium of early-passage and late-passage MSCs (donor #7012). **g** TGFβ1 and PTX3 ELISAs in early-passage and late-passage MSC-EVs from donors # 7075 and # 6015 (n=3). Data are presented as means ± SD. *p < 0.05, ***p < 0.001, ****p < 0.0001 by student's t-test. **h-i** Quantitative band-intensity of western blots in **Figure 6i-k.**

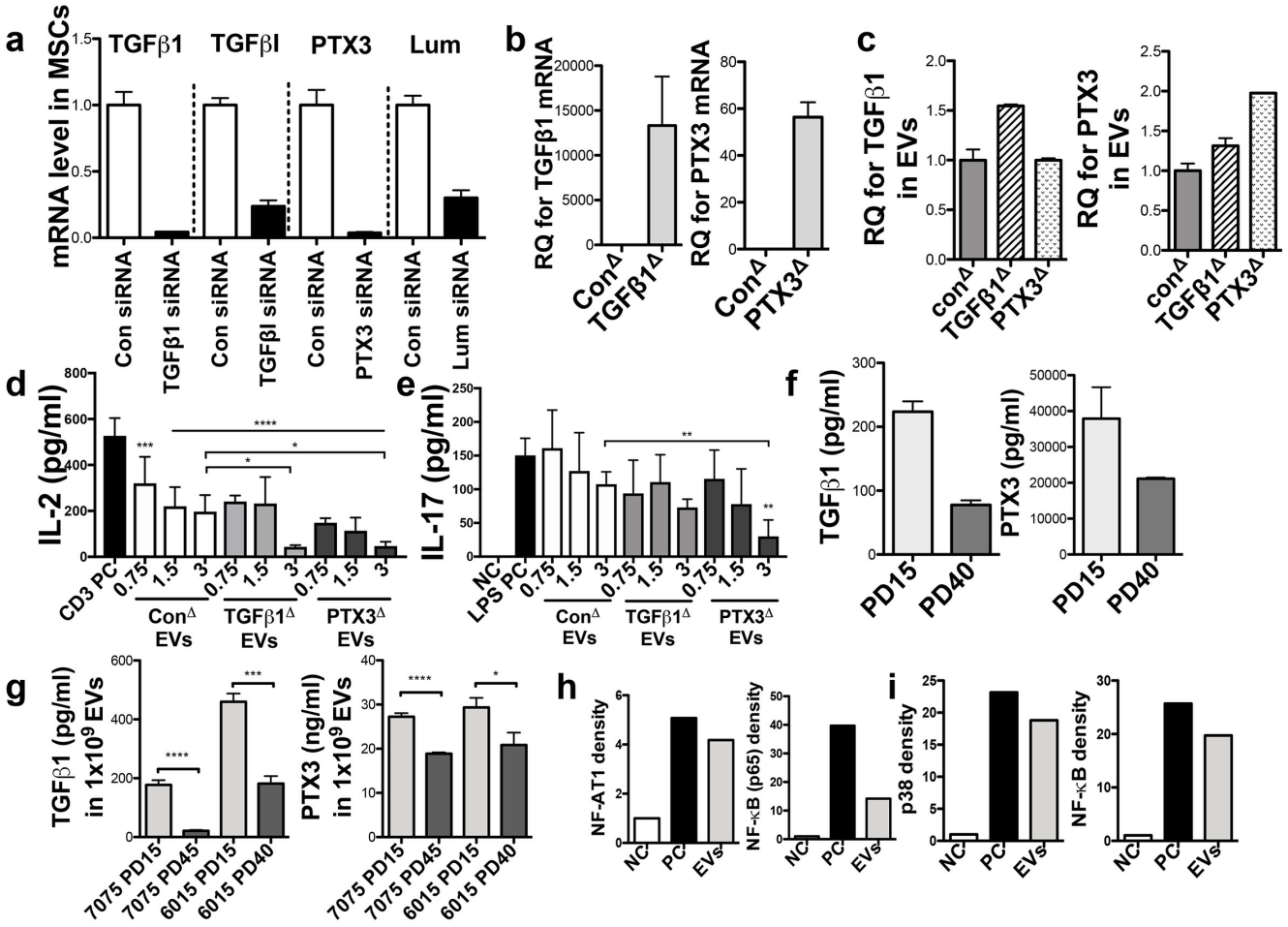

Supplemental Figure 3. Supporting data for the results in Figure 7. a Relative expressions of let-7b and miR-21 in early- and late-passage MSC-EVs from two additional donors #6015 and #7075. **b** Relative expressions of let-7b and miR-21 in PD15 MSCs and let-7b in PD15 MSC-EVs after miRNA inhibitor transfection. **c** TGFβ1 and PTX3 ELISAs with EVs isolated from PD15 MSCs after miRNA inhibitor transfection. All data are presented as means ± SD; *p < 0.05 by Student's t-test or one-way ANOVA with Dunnett's test.

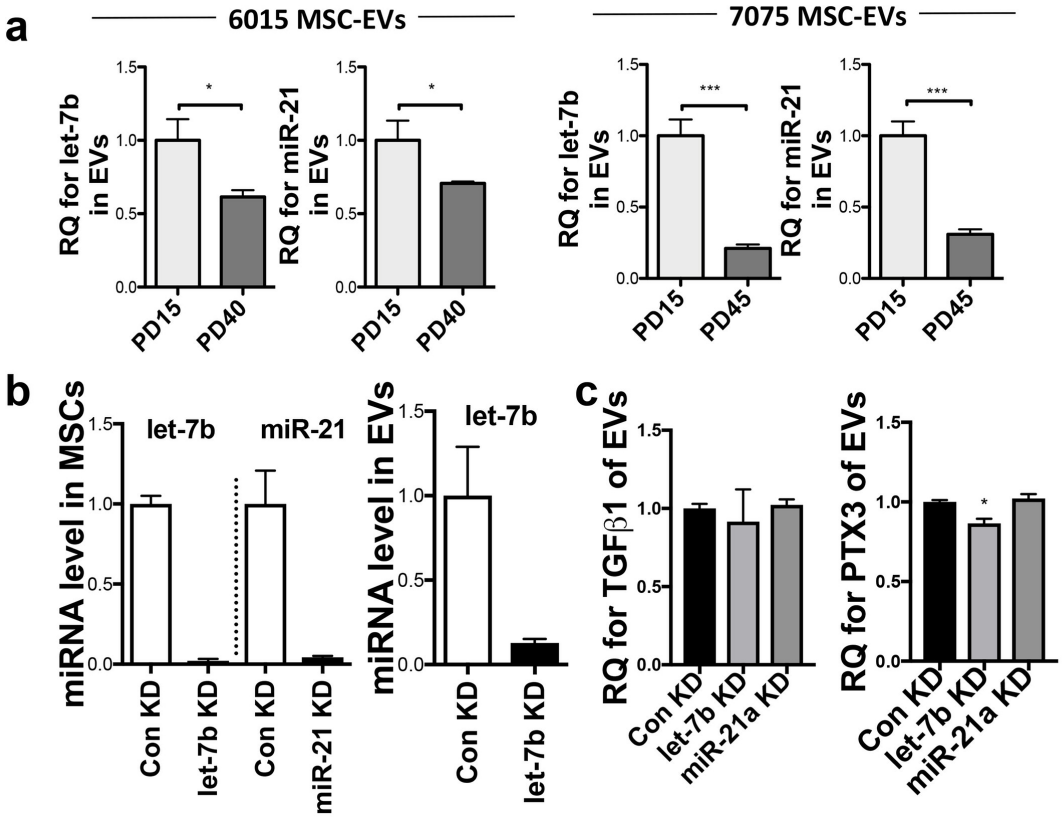

Supplemental Figure 4. Characterization of early-passage and late-passage MSCs (donor #7012). a Flow cytometry analysis with antibodies to the MSC surface markers (CD73, CD90 and CD105), HLAs (human leukocyte antigens) and hematopoietic marker CD34 in early-passage (PD15) and late-passage (PD40) MSCs. **b** Representative images of Oil red O and Alizarin Red staining after adipogenic and osteogenic differentiation induction with PD15 and PD40 MSCs. Both early- and late-passage MSCs expressed the MSC markers, but adipogenic differentiation potential of late passage MSCs was dramatically decreased.

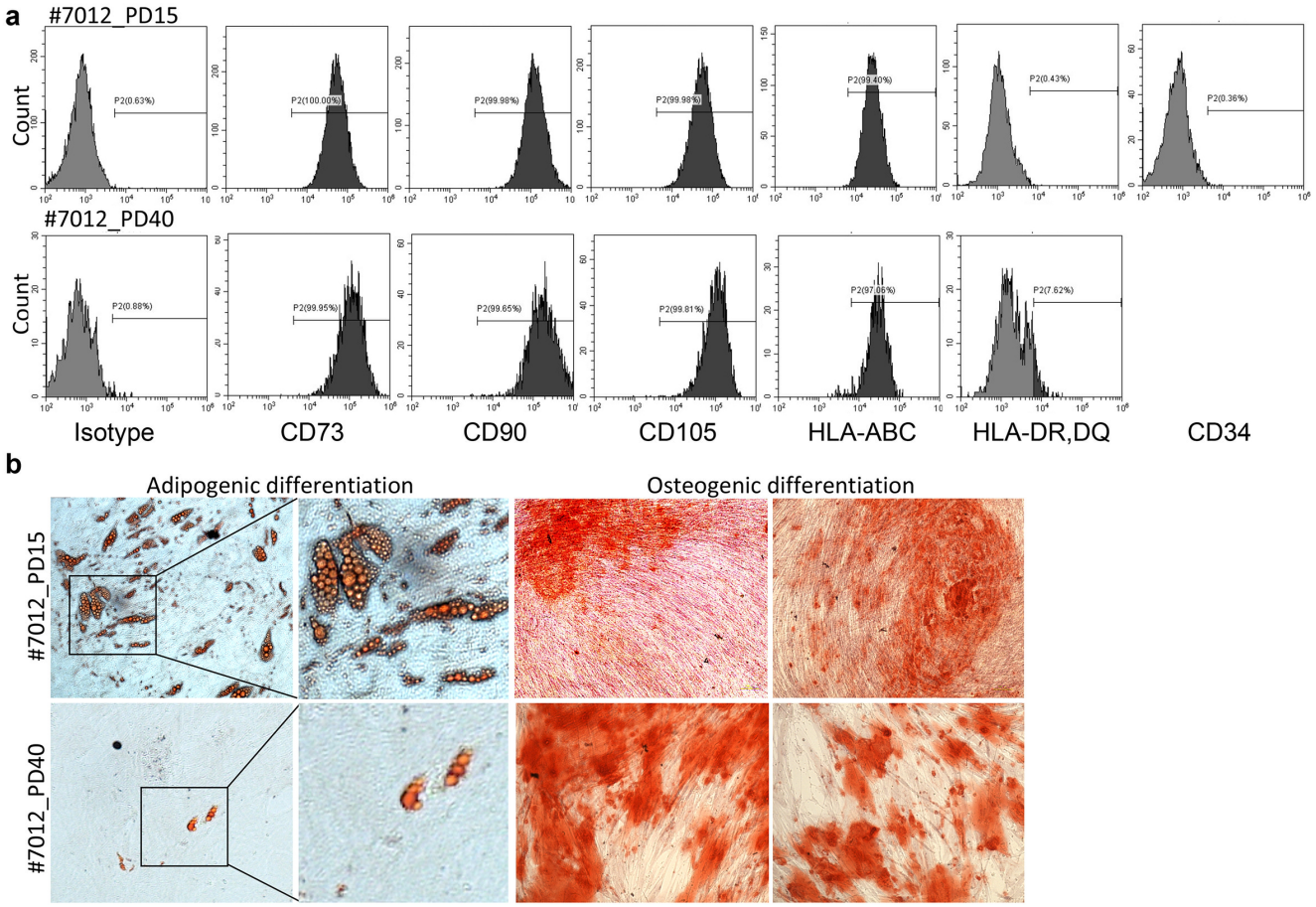

Supplemental Figure 5. Karyotyping of early-passage (PD15) and late-passage (PD35) MSCs (donor #7012). Both early- and late-passage MSCs showed normal diploid genotypes, but some early signs of instability (possible fusions and polyploidization) were also observed in late passage MSCs.